Journal of
Materials Chemistry B

Materials for biology and medicine

Accepted Manuscript

This article can be cited before page numbers have been issued, to do this please use: F. Kaufman, M. David, M. Zaiden, D. Shabat and M. Amiram, *J. Mater. Chem. B*, 2025, DOI: 10.1039/D5TB01334H.

ROYAL SOCIETY OF CHEMISTRY

rsc.li/materials-b

View Article Online
DOI: 10.1039/D5TB01334H

Imparting New Stimuli-Responsive Behaviors in Protein-polymers via Self-Immolative Linker Conjugation

Federico Kaufman[1], Maya David[2], Michal Zaiden[3] Doron Shabat[2] Miriam Amiram[1*]

[1]The Avram and Stella Goldstein Goren Department of Biotechnology Engineering, Ben-Gurion University of the Negev, P.O.B. 653, Beer-Sheva 8410501, Israel.

[2]School of Chemistry, Raymond and Beverly Sackler Faculty of Exact Sciences, Tel-Aviv University, Tel Aviv 69978, Israel.

[3] Department of Chemical Engineering, Ben-Gurion University, Beer Sheva 841050, Israel.

Abstract:

The development of "smart" polymers capable of responding to physiologically relevant stimuli is critical for engineering dynamic sensing and actuation systems that leverage biological signals under specific (patho)physiological conditions. In this study, we present a general and versatile strategy to engineer novel stimuli-responsive behaviors in temperature-sensitive protein-based polymers (PBPs) via site-specific conjugation with self-immolative molecules. Specifically, we developed hydrogen peroxide (H_2O_2)- and β-galactosidase (β-gal)-responsive elastin-like polypeptides (ELPs) and resilin-like polypeptides (RLPs). Using a library of ELPs with varying numbers of conjugation sites, we demonstrate that this approach enables precise modulation of stimulus-responsive phase transitions, providing a tunable temperature window of up to 50 °C for stimuli-controlled phase transition. We further show that incorporation of these responsive ELPs into collagen hydrogels allows for controlled, dose- and time-dependent release of the ELPs, accompanied by stimulus-induced changes in the hydrogel's transparency, and storage and loss moduli. Additionally, we engineered diblock copolymer nanostructures comprising ELP-ELP or RLP-ELP segments for encapsulation and stimulus-triggered release of a hydrophobic model payload (Nile Red) with varying release profiles. Together, these results establish a robust platform for imparting environmentally responsive functionalities to PBPs by integrating recombinant synthesis with chemically triggered actuation, thereby enabling the rational design of adaptive

View Article Online
DOI: 10.1039/D5TB01334H

biomaterials with tunable physicochemical and biological properties for a wide range of biomedical and biotechnological applications.

View Article Online
DOI: 10.1039/D5TB01334H

Introduction

Stimuli-responsive polymers have become essential in the field of biotechnology and biomedical engineering. Such materials are engineered to adjust their properties, structure, or function in response to various stimuli, including light, temperature, pH, or biomolecules (e.g., enzymes) [1, 2]. Leveraging the adaptability of these biomaterials facilitates a wide array of applications, such as drug delivery systems, tissue engineering scaffolds, diagnostics, sensors, and microreactors [3]. Despite the numerous examples of stimuli-responsive polymers, challenges persist in their design and synthesis, particularly in the ability to rationally engineer and precisely control key properties such as morphology, size, stability, the identity of the stimulus, and sensitivity to the desired range of stimulus concentrations [3]. Hence, a great need remains to not only create novel, biocompatible, and programmable stimuli-responsive materials but also to devise a systematic approach for engineering stimuli-responsive behavior and fine-tuning properties and functions to specific applications.

Among the diverse range of polymers, proteins –intricate and precise polymers composed of the 20 amino acid monomers - exhibit unparalleled tailored and diverse responsiveness to stimuli, including but not limited to, ligand binding, post-translational modifications, and protease cleavage, which in turn govern the conformational changes of structural proteins and the solubility and self-assembly of protein-based polymers (PBPs) (and other intrinsically disordered proteins (IDPs)). PBPs such as elastin, resilin, collagen, chitosan, and silk offer versatile and tunable building blocks for the design of coacervates, hydrogels, and nanostructures due to their inherent biocompatibility, biodegradability, and unique mechanical properties [4-8]. Such PBPs are widely exploited in biotechnological and biomedical applications—including tissue engineering and regeneration, drug delivery, immunotherapy, biosensing, and environmental remediation—through the fabrication of tailored hydrogel matrices and nano-to-micro scale structures that mimic natural environments or enable precise therapeutic control [2, 4-6, 9, 10].

To engineer novel stimuli-responsive behaviors in PBPs and their resulting self-assembled structures, we base our design on temperature-responsive PBPs. Specifically, we focus on elastin-like polypeptides (ELPs)—recombinant, temperature-sensitive PBPs that have been widely employed in diverse biomedical and biotechnological applications [11-13]. ELPs consist of a

View Article Online
DOI: 10.1039/D5TB01334H

repeating VPGXG motif, where X, the guest residue, can accommodate both natural and unnatural amino acids. ELPs undergo a thermo-responsive reversible phase transition at their lower critical transition temperature (LCST), denoted as the Tt. Numerous studies have illustrated that compositional hydrophobicity determines the Tt of ELPs (under specific concentration and buffer conditions). The dependence of the Tt on ELP hydrophobicity can be exploited for imparting ELPs with responsiveness to additional stimuli. For instance, responsiveness to light, pH, or ionic strength can be engineered by incorporating the respective stimuli-responsive chemical groups or motifs, which, upon exposure to the stimuli, alter the hydrophobicity of the ELPs [14-17]. The greater the difference in hydrophobicity of the ELP before and after exposure to the stimulus, the wider the temperature range over which the stimulus can be used (isothermally) to influence the ELP phase transition.

In addition to stimuli-responsive phase transitions of single-block ELPs, the genetic fusion of two or more ELP blocks with varying hydrophilicities can drive the formation of self-assembled micelles [18-24]. Additional nanostructure morphologies can be designed by fusing ELPs with resilin-like polypeptides (RLPs)[25], a class of PBPs that exhibit an upper critical solution temperature (UCST), which, like ELPs, can be tuned by altering the hydrophobicity of the RLP sequence [26-30]. Therefore, by modifying the hydrophobicity of the ELP or RLP sequence via stimuli exposure, the Tt, self-assembly, or disassembly can be rationally designed and optimized for a specific application.

Here, we detail a general approach for imparting new stimuli-responsiveness onto temperature-responsive PBPs, such as ELPs and RLPs, inspired by self-immolative polymers, a distinct class of stimuli-responsive materials initially developed by the Shabat group [31, 32]. Such polymers are composed of self-immolative monomers, which are capped by a chemical group that undergoes a triggered intramolecular rearrangement or cleavage reaction upon exposure to a stimulus, leading to the rapid depolymerization or disassembly of the polymer chain from head to tail [33]. We hypothesized that site-specific conjugation of ELPs or RLPs with stimulus-cleavable groups via self-immolative linkers would impart responsiveness across a broad temperature range by inducing a significant change in hydrophobicity before and after stimulus exposure. The incorporation of self-immolative moieties enables pronounced molecular property shifts between the cleaved and uncleaved states, while also offering design flexibility in both linker and caging groups to precisely

View Article Online
DOI: 10.1039/D5TB01334H

control the kinetics and extent of such changes. Compared to conventional self-decomposing systems—such as synthetic polymers or inorganic carriers—such hybrid PBPs offer reduced toxicity and facilitate genetic fusion of bioactive sequences for targeted interactions. In addition, their genetically encoded design allows precise control over amino acid sequence and conjugation sites, enabling fine-tuning of degradation kinetics, structural transitions, and stimuli-responsive behavior.

In this study, we utilize this approach to demonstrate the generation of chemically or enzymatically responsive ELPs by the conjugation of self-immolative linkers capped by an H_2O_2-degradable pinacol-type boronic ester or a β-galactosidase (β-gal)-degradable galactose (molecules **1** and **2**, respectively, Figure 1A). The chosen triggers were selected both based on their biomedical relevance in various diseases (e.g., cancer, inflammation, and aging [34, 35]) and their representation of distinct stimulus classes—chemical versus enzymatic, and small molecule versus macromolecular protein—enabling a comprehensive investigation of how diverse trigger types modulate the behavior in various PBP configurations. The functionalization of molecules **1** and **2** with an azide group enables their site-specific, bio-orthogonal conjugation to alkyne groups incorporated into ELPs via an unnatural amino acid (uAA), 4-propargyloxy-L-phenylalanine (pPR) (Figure 1) [36]. We produce libraries of ELPs conjugated to varying numbers of **1** or **2** and analyze their sequence-chemical composition-function behavior. We demonstrate that the cleavage of the head group and subsequent removal of the self-immolative linker in compounds **1** or **2** triggers significant changes in the X-guest residue position and, hence, ELP hydrophobicity. By controlling the ELP sequence and the number and positions of conjugation sites, ELP conjugates can be used to induce H_2O_2- or β-gal-responsive phase transitions in solution at tunable temperature windows. In turn, these stimuli-responsive ELPs can facilitate controlled release and changes in optical density, storage, and loss modulus within collagen-ELP hydrogels. Finally, we demonstrate that this approach can be extended to the design of diverse nanostructures composed of ELP–ELP and ELP–RLP diblock copolymers, capable of stimuli-responsive disassembly accompanied by the release of encapsulated cargo.

View Article Online
DOI: 10.1039/D5TB01334H

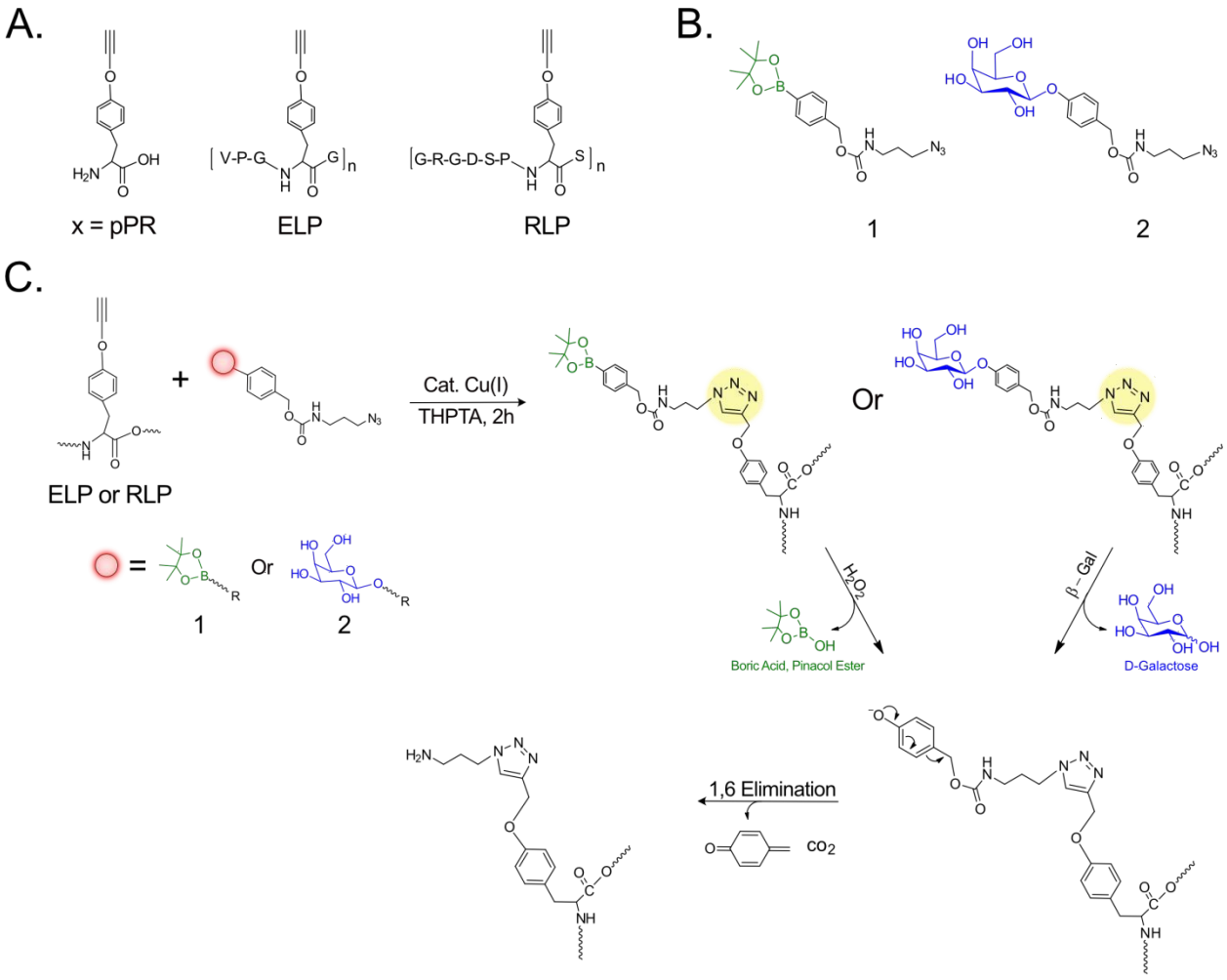

Figure 1. (A) Chemical structure of 4-propargyloxy-L-phenylalanine (pPR) and schematic illustration of an ELP and RLP repeat units functionalized with alkyne groups via pPR incorporation. (B) Chemical structures of molecules **1** and **2**. (C) Conjugation of molecules **1** or **2** to ELP or RLP via formation of a triazole ring (yellow circle) through a click chemistry reaction. (D) Mechanism of the stimuli-responsive cleavage of molecules **1** and **2**, illustrated as conjugates to an ELP via pPR. Both reactions proceed through a self-immolative 1,6-elimination, resulting in the same final product.

View Article Online
DOI: 10.1039/D5TB01334H

Results and Discussion

Design of single-block ELP-conjugates for stimuli-responsive phase transition.

To examine the effect of conjugation and subsequent stimuli-responsive cleavage of **1** [37] or **2** **(**see Supplementary Information for synthetic procedures**)** on the phase-transition behavior of ELPs, we utilized our previously designed set of ELP variants [14, 38] which are composed of 60 pentapeptides having glycine or alanine amino acids alternating in the X-guest residue position and 0, 2, 4, 6 or 10 TAG codons distributed evenly along the ELP guest residue positions [termed ELP_{60}WT, ELP_{60}(TAGx2), ELP_{60}(TAGx4), ELP_{60}(TAGx6), and ELP_{60}(TAGx10), respectively, Supplementary Table S1]. We selected this set of hydrophilic ELPs as hosts for the incorporation of the alkyne-bearing uAA 4-propargyloxy-l-phenylalanine (pPR) [36] at the TAG codons, and subsequent conjugation of **1** or **2**, since the hydrophobic uAAs and self-immolative molecule were expected to reduce the Tt when incorporated in multiple sites in the ELPs. Throughout the paper, proteins expressed from the above-mentioned ELP genes are named according to the number and identity of the molecule incorporated in the TAG codons. For example, ELP_{60}(**1**×6) is the protein conjugate of ELP_{60}(**pPR**×6) with molecule **1**, which in turn is the product of the ELP_{60}(TAGx6) gene.

We first produced and conjugated this set of ELPs to molecules **1** or **2**, and examined the temperature-dependent absorbance of the ELPs conjugates. As expected, increasing the number of conjugated molecules increased the overall ELP hydrophobicity, thus decreasing its Tt (compared with bare, un-conjugated ELPs). In addition, regardless of the number of conjugated molecules per ELP, the conjugation of **1** resulted in an ELP with a lower Tt than ELP conjugated to **2** (Figure 2), as the former is more hydrophobic than the latter (calculated ClogP of 1.77 and -1.58 for the head groups of molecules **1** and **2**, respectively). Thus, an ELP with ten sites for conjugation (ELP_{60}(**pPR**x10)) exhibited a Tt above 10 ^{0}C when conjugated to **2**, whereas conjugation with **1** generated a Tt below the examined temperature range (data not shown). Similarly, an ELP with four sites for conjugation (ELP_{60}(**pPR**x4)) exhibited a Tt above 90 ^{0}C when conjugated to **2** in PBS, and was therefore determined in PBS supplemented with 1M NaCl, whereas conjugation with **1** generated a Tt within the examined temperature range (in PBS). The extent of conjugation was evaluated by intact mass spectrometry, which revealed near-complete conjugation of the ELPs with molecule **1**. In contrast, ELPs conjugated with molecule **2** also exhibited peaks corresponding

View Article Online
DOI: 10.1039/D5TB01334H

to n–1 conjugated species, regardless of variations in reaction conditions such as time, temperature, or fold excess of the azide-molecule (Supplementary Table S2 and Figure S1-2). This discrepancy may be attributed to the relatively higher hydrophilicity or larger hydrodynamic size of molecule **2** compared to molecule **1**.

Upon incubation with the appropriate stimulus (i.e., 1 mM H_2O_2 for conjugates with molecule **1** or 5 mg/ml β-gal for conjugates with molecule **2**), cleavage of the head group and self-immolative linker generated a significant increase in the hydrophilicity of the ELPs. This was evidenced by the fact that after stimulus exposure, all ELPs [except for the most hydrophobic protein ELP_{60}(**pPR**×10)] exhibited a Tt above the observed temperature range (>90 °C) in PBS. Consequently, stimulus exposure generated a difference in the Tt (ΔTt) as large as ~ 50 or 40 °C for ELPs conjugated with six molecules of **1** or **2,** respectively (Figure 2, Supplementary Table S3). As expected, exposure of the control (bare, unconjugated ELP) to either stimulus had little effect on the transition profile (Supplementary Figure S3). The observed minor effect can be attributed to slight variations in the concentration of the ELP and the presence of co-solutes (i.e., β-gal). Another factor influencing the transition profile is the concentration of the triggering molecules. Lower concentration of the stimulus or shorter incubation times can result in incomplete cleavage, leading to a polymer mixture with intermediate hydrophobicity, having some remaining un-cleaved molecules. This effect is evident when less than a 1:1 molar equivalent of H_2O_2 is added to ELP_{60}(**1**×6) or when ELP_{60}(**2**×10) is subjected to a shorter incubation with β-gal (Supplementary Figure S4).

Overall, the phase transition profiles of the ELP conjugates confirm that the conjugation of molecules **1** and **2** increases the hydrophobicity of the ELP, which decreases the ELP Tt. Furthermore, the greater the hydrophobicity of the conjugated molecule, the lower the ELP's Tt and the larger the ΔTt generated upon stimulus exposure. These trends confirm that ELP conjugates of this type adhere to the established guidelines for predicting and tuning the ELP phase transition temperature using both natural and unnatural chemical groups [26, 39], enabling the rational design of stimuli-responsive ELP variants with a predetermined transition temperature both before and after stimulus exposure, and thus a tunable working temperature window.

View Article Online
DOI: 10.1039/D5TB01334H

The well-established dependence of the ELP Tt on its hydrophobicity has been leveraged to design a variety of stimuli-responsive ELPs. For example, pH-responsive ELPs have been engineered by introducing charged residues at the guest position, resulting in a ~60 °C shift in the Tt when the pH is varied from 3 to 8 [17, 40]. In another example, the incorporation of calcium-binding short peptide motifs enabled the design of calcium-responsive ELPs, exhibiting a ~40 °C shift in transition temperature upon the addition of 10 μM calcium [41]. To enable access to additional types of stimuli, uAA incorporation can be used to incorporate synthetic stimuli-responsive groups using the protein translation machinery. In previous work, we demonstrated that site-specific incorporation of uAAs bearing azobenzene or its derivatives enabled the generation of light-responsive ELPs, which exhibited up to a 45 °C change in Tt upon irradiation with different wavelengths [14, 15]. Building on this strategy, we now show that the site-specific conjugation of self-immolative molecules to bio-orthogonal chemical groups incorporated as uAAs, can induce pronounced shifts in the Tt in response to specific chemical or enzymatic stimuli. Notably, this approach offers enhanced versatility: the stimulus can be modified by altering the self-immolative head group, and post-purification conjugation eliminates the need for stimulus-specific translational machinery. However, compared to direct incorporation of uAAs, post-translational conjugation requires additional purification steps and, for certain molecules—such as compound 2—may result in incomplete conjugation. With future scale-up for clinical applications in mind, we demonstrated that high-performance translation machinery enables the efficient production of PBPs, such as ELPs, containing multiple uAAs at high yields [26]. While expression has so far been demonstrated only at a small scale, further optimization using industrial-scale expression systems is expected to enhance production efficiency.

Both H_2O_2- and β-gal-responsive ELPs exemplify the concept of smart materials that can respond to endogenous chemical or biological stimuli and adapt to the biochemical environment. H_2O_2 is a reactive oxygen species (ROS) that plays a critical role in cellular signaling and oxidative stress. Elevated levels of H_2O_2 are commonly associated with pathological conditions such as cancer, inflammatory diseases, and cardiovascular diseases [35, 42]. Additionally, H_2O_2 can be generated in a controlled manner through chemical reactions, for example, for glucose-responsive diabetes treatment [43]. β-Gal is commonly overexpressed in certain disease states, particularly in senescent cells, which are often found in cancer and age-related conditions [44]. As a result, β-Gal can be

View Article Online
DOI: 10.1039/D5TB01334H

exploited for targeted delivery to senescent cells [45-47]. However, beyond the potential utility of these specific stimuli, this straightforward and versatile approach can be applied for the design of stimuli-responsive polymers by leveraging a wide range of both established and unexplored self-immolative molecules, which can be similarly employed to introduce new stimuli-responsive behaviors across broad and tunable temperature ranges. Previously developed self-immolative molecules have been designed to respond to various biological, chemical, and physical stimuli, such as enzymes, proteases, hydrogen sulfide, pH changes, Pd(0), fluoride ions, and UV or visible light [48, 49]. Additional cleavable head groups could be utilized in this context, including azobenzene and its derivatives, which are sensitive to hypoxia and certain enzymes, the 2-aza-Cope formaldehyde-reactive trigger, and the neuraminidase substrate N-acetylneuraminic acid [26-28]. These molecules could potentially integrate with self-immolative linkers for imparting ELPs with novel stimuli-responsive functions relevant to various physiological conditions. Lastly, despite the utility of self-immolative molecules in creating synthetic degradable polymers, ELPs offer a distinct advantage, especially in biomedical applications, since synthetic polymers and their degradation products are often toxic [49], while ELPs are both biodegradable and non-immunogenic [11].

View Article Online
DOI: 10.1039/D5TB01334H

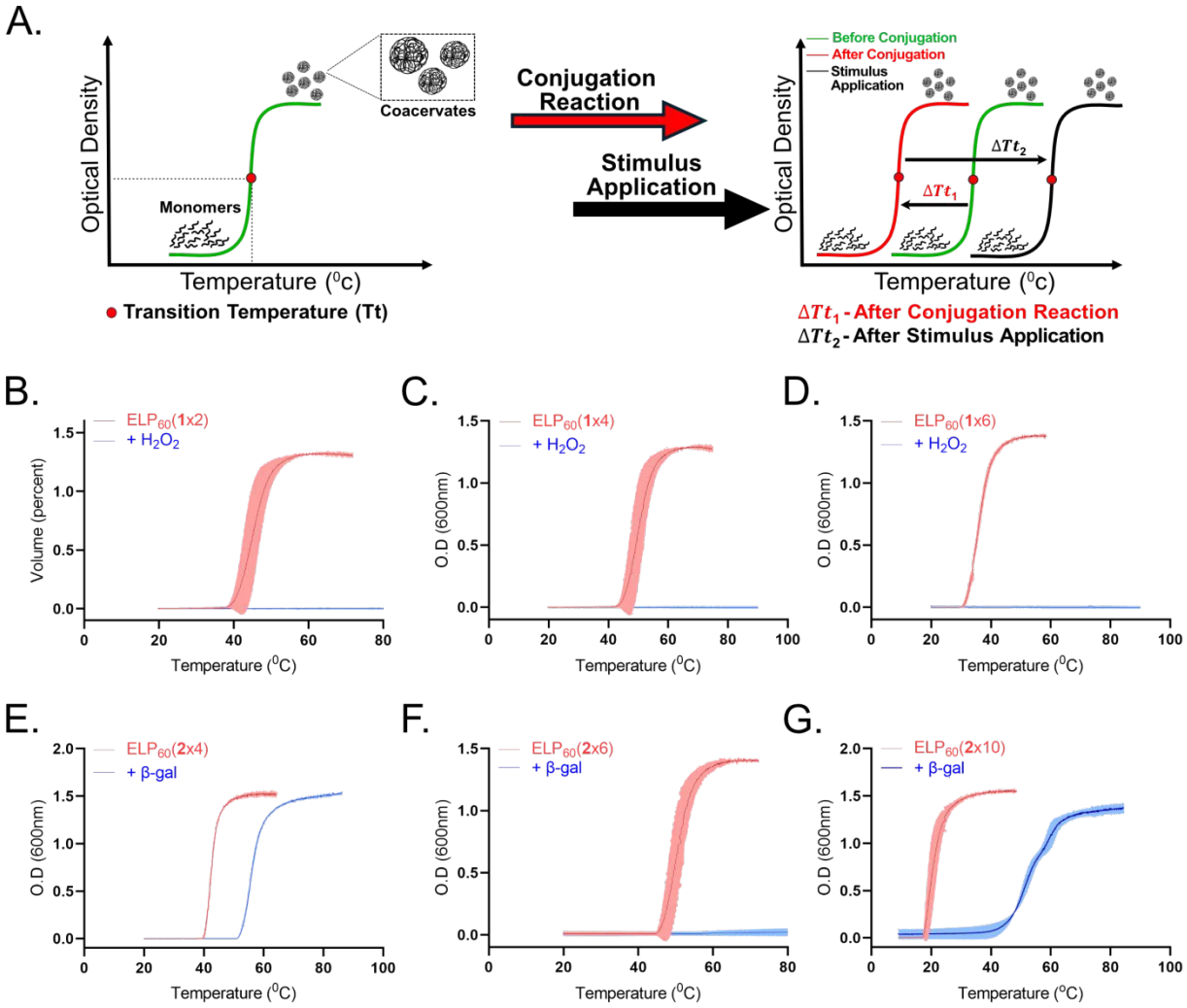

Figure 2. (A) Schematic representation of the change in the turbidity profile of the ELP upon conjugation to the self-immolative linkers and subsequent stimulus exposure. Turbidity profiles as a function of temperature before and after exposure of the respective proteins (20 μM in PBS unless otherwise noted) to the stimulus: (B) ELP_{60}(**1**×2) (supplemented with 1 M NaCl), (C) ELP_{60}(**1**×4), (D) ELP_{60}(**1**×6) - incubated with 1 mM H_2O_2. (E) ELP_{60}(**2**×4) (supplemented with 1 M NaCl), (F) ELP_{60}(**2**×6), (G) ELP_{60}(**2**×10) - supplemented with 5 mg/ml β-gal. Error bars indicate average values ± SD.

View Article Online
DOI: 10.1039/D5TB01334H

Engineering stimuli-responsive ELP-collagen hydrogels

Hydrogels are soft materials that absorb and retain large volumes of water without dissolving, due to their three-dimensional crosslinked polymer network structure [10]. Previous studies have demonstrated that the temperature-responsive phase transition of ELPs in solution can be harnessed to modify the properties of hydrogels, whether composed solely of ELPs or in combination with other natural or synthetic biopolymers [11, 50-52]. To impart stimuli-responsive behavior to hydrogels through ELP incorporation, we based our design on previously described hydrogels consisting of a mixture of ELP and collagen. In this approach, collagen-mediated hydrogel formation at 37 °C eliminates the need for crosslinkers and reduces the amount of ELP required to promote gelation [53-55].

To evaluate the stimuli-responsive behavior of hydrogel-embedded ELPs, we selected two single-block ELPs with Tt below 37 °C after conjugation—specifically, ELP_{60}(**1**×6) and ELP_{60}(**2**×10)—and generated hydrogels composed of an ELP:collagen ratio 1.5:1 mg/ml (60 μM ELP) and 0.8:1 mg/ml (30 μM ELP), using ELP_{60}(**1**×6) and ELP_{60}(**2**×10), respectively. In both cases, incubation of the mixture (or collagen-only control) in PBS at 37 °C for 2 hours was sufficient to form the hydrogels (Figure 3A). ELP-containing hydrogels exhibited significantly higher opacity at 37 °C (above the ELPs' Tt) than the collagen-only control due to the ELP phase transition at this temperature, as was previously demonstrated for hydrogels composed of ELP and PEG [50]. Incubation of the hydrogels in PBS solutions with varying concentrations of the respective stimuli resulted in a reduction in hydrogel opacity consistent with the observed increase of the Tt and solvation of these ELPs upon stimulus exposure (Figure 3A), with the kinetics and magnitude of this effect increasing with the application of higher concentrations of H_2O_2 or β-gal (Figure 3B-C). The rate of optical density reduction is faster after application of H_2O_2 compared to β-gal, suggesting that the diffusion rate of the larger β-gal enzyme into the hydrogel is slower than that of H_2O_2 molecule, exemplifying the distinct activation dynamics of chemical versus enzymatic stimuli for ELPs embedded in hydrogel systems. Moreover, SDS-PAGE analysis of samples collected from the surrounding solution at different time points up to 24 h reveals that ELP dissolution upon stimulus-responsive cleavage of compounds **1** or **2** prompts its release from the hydrogel in a time and stimulus-concentration-dependent manner. In contrast, significantly smaller

View Article Online
DOI: 10.1039/D5TB01334H

amounts of ELP were released after incubation of the hydrogel in PBS for the same durations (Figure 3D-E and Supplementary Figure S5).

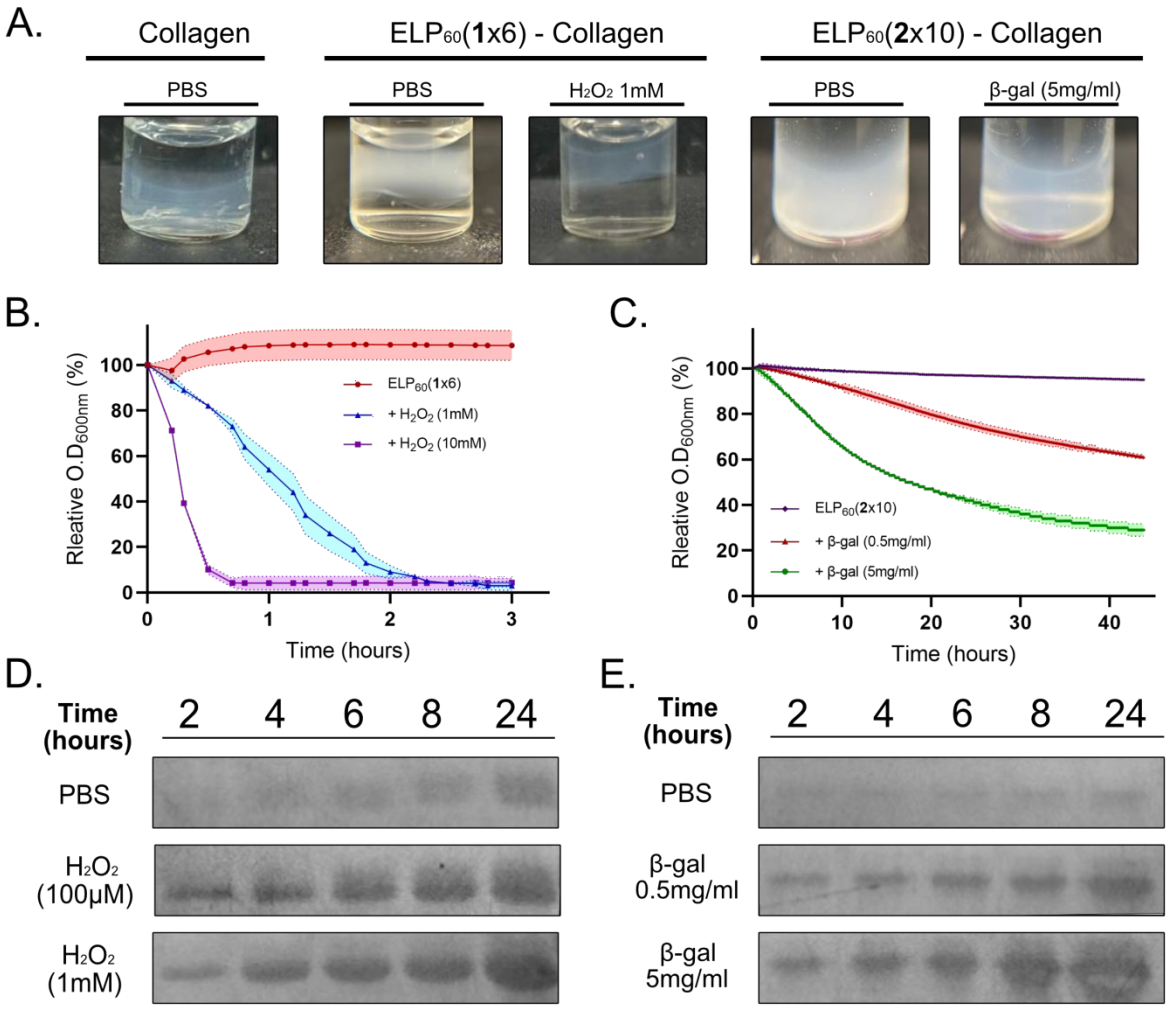

Figure 3. (A) Images of hydrogels composed of collagen, collagen and ELP$_{60}$(**1**×6), and collagen and ELP$_{60}$(**2**×10) as indicated. All hydrogels were incubated for 24 h in PBS with or without the respective stimulus as indicated above the image. (B-C) Time course analysis of the turbidity of hydrogels composed of collagen and (B) ELP$_{60}$(**1**×6) or (C) ELP$_{60}$(**2**×10) incubated in PBS or with varying amounts of H_2O_2 or β-gal, respectively. (D-E) SDS-PAGE of the ELP released from

View Article Online
DOI: 10.1039/D5TB01334H

hydrogels composed of collagen and (D) ELP_{60}(**1**×6) or (E) ELP_{60}(**2**×10) at varying time points after incubation in PBS or with varying amounts of H_2O_2 or β-gal, respectively.

We next investigated the effect of coacervate dissolution and ELP release on the mechanical properties of ELP–collagen hydrogels. The storage modulus (G′), representing elastic behavior, and the loss modulus (G″), representing viscous behavior, were measured as functions of oscillation frequency (Figure 4A-B, Table 1). This analysis revealed that the incorporation of ELP(**1**×6) or ELP(**2**×10) in the collagen hydrogels increased the observed G′ values by approximately 55% and 30% respectively, while only a minor increase was observed in G″ (at an oscillation frequency of 1 $rad \cdot s^{-1}$). This is likely due to standard measurement variability, as the change is within the range of the standard deviation (for ELP **1**x6), as compared with collagen-only hydrogels (Supplementary Figure S5). In contrast, 24 h after addition of the respective stimulus (1 mM H_2O_2 for ELP **1**x6 and 5 mg/ml β -gal for ELP **2**x10), both ELP–collagen hydrogels exhibited a decrease in both G' and G''' approximating the values measured for hydrogels composed of only collagen measured by us and others using similar protocols [56, 57] (Supplementary Figure S6).

View Article Online
DOI: 10.1039/D5TB01334H

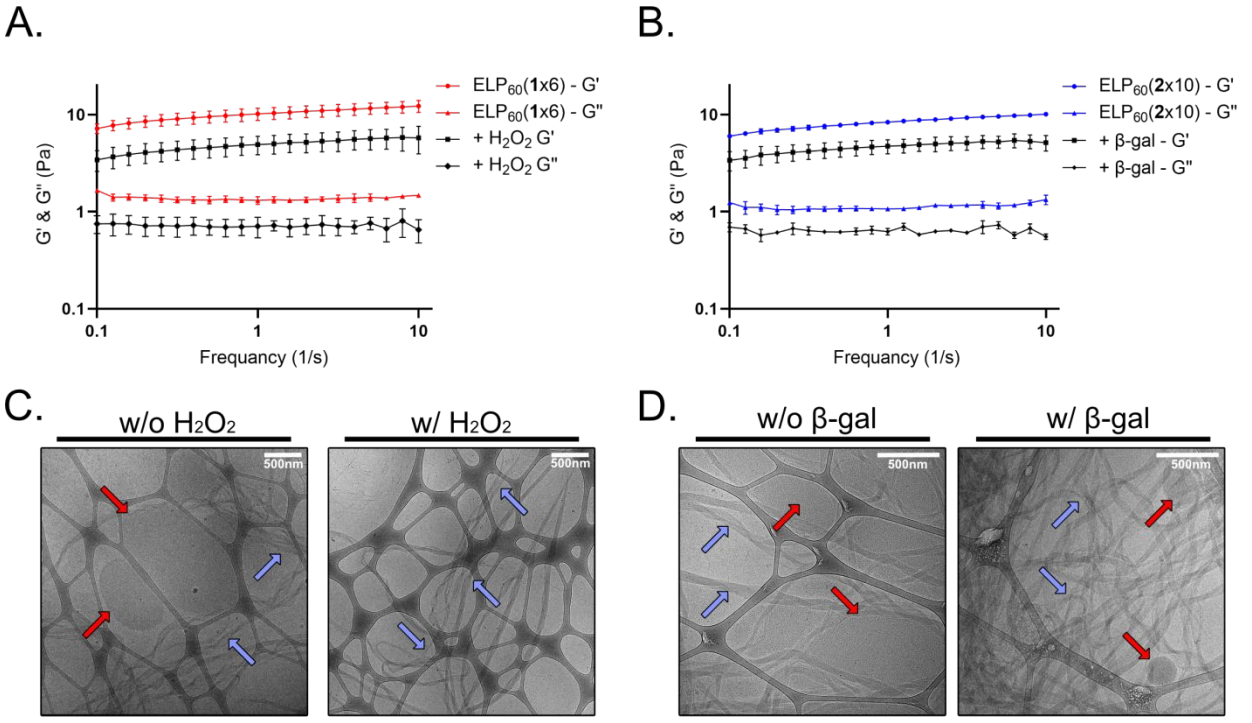

Figure 4. (A-B) Frequency sweep tests of the (A) ELP_{60}(**1**x6)-Collagen and (B) ELP_{60}(**2**x10)-Collagen hydrogels. The frequency varied from 0.1 to 10 rad s−1 with a constant strain of 1% for the frequency sweep detections. Error bars indicate average values ± SD. (C) Cryo-TEM images of hydrogels composed of collagen and ELP_{60}(**1**×6), 24 h after incubation with PBS or 1 mM H_2O_2. (D) Cryo-TEM images of hydrogels composed of collagen and ELP_{60}(**2**×10), 24 h after incubation with PBS or 5 mg/ml β-gal. Red arrows indicate aggregates and blue arrows indicate collagen fibers, scale bar – 500nm.

Table 1. Storage (G′) and loss (G″) modulus values of Collagen and ELP-Collagen hydrogels under different conditions.

Hydrogels	PBS		w/ H_2O_2		w/ β - gal	
	G' (Pa)	G'' (Pa)	G' (Pa)	G'' (Pa)	G' (Pa)	G'' (Pa)
ELP (**1**x6) - Collagen	10.2 ± 1.4	1.3 ± 0.1	4.9 ± 1.1	0.7 ± 0.2	----------	
ELP (**2**x10) - Collagen	8.4 ± 0.2	1.06 ± 0.01	----------		4.7 ± 0.8	0.62 ± 0.04

View Article Online
DOI: 10.1039/D5TB01334H

To verify that the observed decrease in G′ and G″ was not due to direct effects of H_2O_2 or β-gal on the hydrogel's physical properties, control collagen-only hydrogels were incubated with the respective stimuli for 24 hours. The measured G′ and G″ values remained unchanged within statistical error, confirming that the decrease in mechanical strength is due to ELP dissolution and diffusion from the hydrogel (Supplementary Figure S6). In addition, SDS-PAGE analysis of collagen incubated for 24 h with up to 10 mM H_2O_2 or 5 mg β-gal showed no detectable collagen degradation, further confirming that the stimuli exert their effects specifically on the ELP without compromising the collagen matrix (Supplementary Figure S7). Finally, cryo-TEM images of the hydrogels without exposure to their respective stimuli (after 24 h incubation in PBS) confirm the presence of ELP aggregates in the areas between the collagen fibers. In contrast, 24 h after exposure to H_2O_2, no aggregates can be seen in the image, whereas few aggregates can still be observed in the β-gal-responsive hydrogels, consistent with their respective release profiles (Figure 4C-D).

The design of protein-based hydrogels whose physical and mechanical properties can be modulated by environmental stimuli holds promise for a range of applications, including drug delivery, tissue engineering, and sensor-actuator systems [10, 11, 52, 58, 59]. Here, we demonstrate a simple and generalizable concept whereby integrating H_2O_2 and β-gal-responsive ELPs into collagen-based hydrogels allows for manipulation of the gels' optical and physical properties and the release of the ELPs from the hydrogel. Since the ELP phase transition behavior is retained in ELP conjugates and ELP-fusion proteins [11], similar ELP-collagen hydrogels can be adapted for the stimuli-responsive release of ELP fusions with small molecules, peptides, and proteins. Notably, because the ELP and collagen are in solution at room temperature and form a gel upon warming to 37 °C, they are also suitable as in situ-gelling injectable hydrogels [53].

Previous analyses of hydrogels composed of ELP and collagen have shown that incorporating ELPs enhances the elastic modulus, tensile strength, and toughness of the hydrogels compared to those made solely of collagen. This improvement has been attributed to the reinforcement of the collagen network by ELP aggregates and was found to vary with the ELP-to-collagen ratio [54, 55, 60]. Although the composition and preparation of hydrogels in prior studies differed from those in the present work, supplementation with ELPs similarly enhanced their mechanical properties. In our system, however, we were uniquely able to reinforce the link between ELP

View Article Online
DOI: 10.1039/D5TB01334H

aggregates and mechanical enhancement by demonstrating that their presence increases both the elastic and loss moduli of the hydrogel, and that their dissolution leads to a decrease in the elastic and loss modulus. Future studies will aim to elucidate and tune the effects of ELP sequence, composition, and concentration, as well as the impact of stimuli-responsive ELP dissolution on additional hydrogel properties, as well as the ELP release profile.

Designing nanostructures for stimuli-responsive disassembly

A common strategy for designing self-assembling natural and synthetic polymers involves fusing two or more polymer blocks with (sufficiently) different hydrophilicities. Consistent with this approach, numerous studies have shown that genetically linking two ELP blocks with varying hydrophilicities can lead to the formation of self-assembled micelles [18-24]. Moreover, work by us and others has demonstrated that RLP-ELP block copolymers can self-assemble into a broader range of morphologies, including elongated, worm-like micelles [27-29]. Motivated by these studies, we aimed to investigate whether conjugating molecules **1** or **2** to the ELP or RLP blocks in diblock copolymers could promote their self-assembly by enhancing the hydrophobicity contrast between the two blocks, with subsequent exposure to stimuli triggering disassembly through increased hydrophilicity upon cleavage of the hydrophobic moieties.

We first fabricated ELP-ELP diblocks such that self-assembly will be prompted by generating a sufficiently hydrophobic ELP block through the conjugation of molecules **1** or **2**, thereby promoting nanostructure formation. Conversely, exposure to stimuli and cleavage of the hydrophobic groups would trigger disassembly due to the resulting increase in the hydrophilicity of this ELP block (Figure 5A). To this end, we followed previously established guidelines for designing ELP diblock copolymers, which have been shown to self-assemble into spherical micelles at hydrophilic-to-hydrophobic block ratios between 1:2 and 2:1 [14, 18]. Specifically, the ELP diblock, termed ELP_{60}(WT)-ELP_{60}(TAGx10) consist of the gene for ELP_{60}(WT), having 60 pentapeptides with alternating alanine and glycine in the X guest-residue position (the hydrophilic block), fused at the genetic level to the gene for ELP_{60}(TAGx10) (the hydrophobic block), thus setting a 1:1 hydrophilic:hydrophobic block ratio. We then expressed and conjugated the proteins

View Article Online
DOI: 10.1039/D5TB01334H

to generate ELP_{60}(WT)-ELP_{60}(**1**×10) and ELP_{60}(WT)-ELP_{60}(**2**×10) and characterized their phase transition and self-assembly behavior.

The temperature-dependent absorbance profiles of the ELP diblocks confirmed that, similar to single-block ELPs—where conjugation of molecules **1** or **2** occurs at sites distributed along the entire sequence—asymmetric conjugation to only one ELP segment also led to an increase in overall hydrophobicity, resulting in a decreased Tt (Figure 5B and E). However, the ΔTt observed upon stimulus exposure in the diblock ELPs is smaller than that seen in the single-block ELPs. This difference is likely attributable to the larger size of the diblocks—twice that of the single-block counterparts—which reduces the relative impact of each conjugation/cleavage event on the overall polymer behavior. This observation, consistent with trends seen when increasing the number of conjugation sites in single-block ELPs, suggests that ΔTt is influenced not only by the number of conjugated groups but by their proportion relative to the ELP's molecular weight. Interestingly, the Tt of ELP_{60}(WT)-ELP_{60}(**2**×10) was slightly lower than that of ELP_{60}(WT)-ELP_{60}(**1**×10), despite the higher hydrophilicity of the former. This behavior contrasts with that observed in single-block ELPs, where increased hydrophobicity of the conjugated molecule results in a lower Tt. The observed trend is characteristic of nanostructure formation, in which the apparent Tt is governed not only by global hydrophobicity, but by the local ELP concentration within the self-assembled state. Indeed, dynamic light scattering (DLS) analysis confirms nanostructure formation at a physiologically relevant temperatures for both ELP_{60}(WT)-ELP_{60}(**1**×10) and ELP_{60}(WT)-ELP_{60}(**2**×10) (Supplementary Figure S8), with a critical micelle concentration (CMC) <5 and ~20 μM, respectively (Figure 5C and F). Moreover, nanostructure disassembly can be observed upon incubation with the respective stimulus, the extent of which increases with H_2O_2 concentration or incubation time with β-gal (Figure 5D and G). Furthermore, while incubation with 1 mM H_2O_2 results in complete disassembly within 1 hour, exposure to 100 μM H_2O_2 produces a slower disassembly profile, with near-complete disassembly occurring after 4 hours (Supplementary Figure S9A). Conversely, nanostructures exposed to 10 μM H_2O_2 or in PBS alone remain stable for at least 24 h (Supplementary Figure S9B). Although the application of 100 μM H_2O_2 is insufficient (by molar basis) for complete cleavage of the trigger groups (as indicated also in Supplementary Figure S4A), this data indicates that partial cleavage can induce a sufficiently large change in the hydrophilicity of the hydrophobic block to promote disassembly.

View Article Online
DOI: 10.1039/D5TB01334H

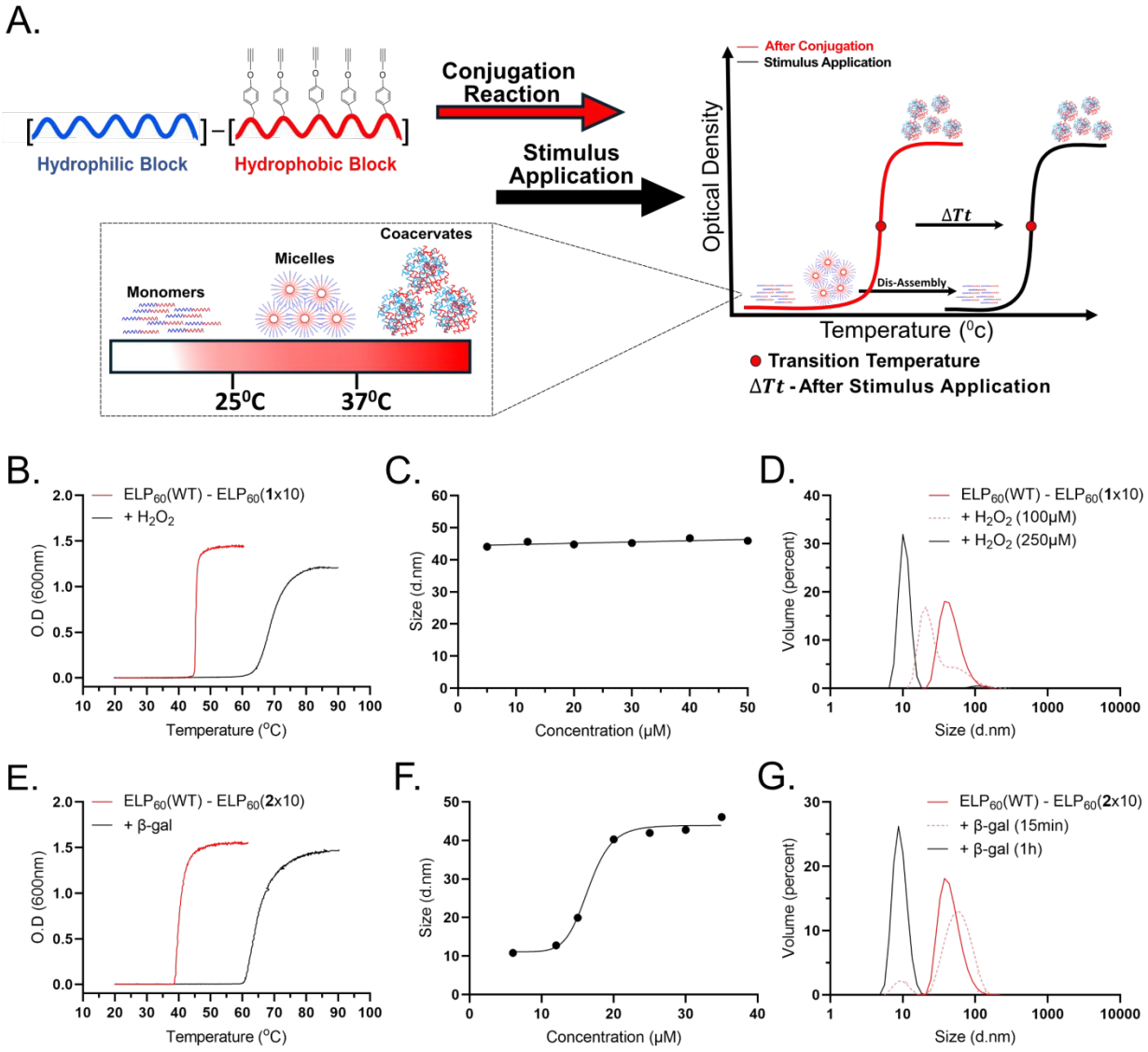

Figure5. (A) Schematic illustration of turbidity and self-assembly changes in ELP_{60}(WT)–ELP_{60}(**pPR**×10) upon conjugation with molecule **1** or **2** and stimulus exposure. **(**B**)** Turbidity profiles as a function of temperature for ELP_{60}(WT)–ELP_{60}(**1**×10) before and after exposure to 1 mM H_2O_2 (12 μM in PBS). **(**C**)** Hydrodynamic diameter as a function of concentration for ELP_{60}(WT)–ELP_{60}(**1**×10). **(**D**)** Hydrodynamic diameter of ELP_{60}(WT)–ELP_{60}(**1**×10) before and 1 h after exposure to 100 or 250 μM H_2O_2 (12 μM in PBS, 37 °C). **(**E**)** Turbidity profiles as a function of temperature for ELP_{60}(WT)–ELP_{60}(**2**×10) before and 1 after incubation with 5 mg/mL β-gal (12 μM in PBS). **(**F**)** Hydrodynamic diameter as a function of concentration for ELP_{60}(WT)–ELP_{60}(**2**×10). **(**G**)** Hydrodynamic diameter of ELP_{60}(WT)–ELP_{60}(**2**×10) before and after 5 mg/mL β-gal for 15 min or 1 h (25 μM in PBS, 37 °C).

View Article Online
DOI: 10.1039/D5TB01334H

We next investigated whether additional nanostructure morphologies could be designed using RLP-ELP diblock copolymers. For this purpose, we employed an RLP-ELP diblock architecture consisting of 60 repeats of the GRGDSPYS (resilin-like) peptide, in which 18 of the 60 tyrosine residues were replaced with TAG codons to allow for pPR incorporation. This RLP block was also genetically fused to a hydrophilic ELP block, ELP_{60}(WT), composed of 60 repeats of the VPGXG pentapeptide, with glycine and alanine alternating in the X position, with the RLP segment serving as the hydrophobic block (Figure 6A). This design was selected based on previous findings showing the ability of this construct to self-assemble into a range of nanostructures, depending on the hydrophobicity of the RLP block, including elongated, worm-like micelles [29]. We then expressed and conjugated the proteins to generate RLP_{60}(**1**×18)-ELP_{60}(WT) and RLP_{60}(**2**×18)-ELP_{60}(WT) and characterized their phase transition and self-assembly behavior.

Temperature-dependent absorbance measurements of the RLP-ELP diblocks confirmed that conjugation of molecules **1** or **2**, and their subsequent cleavage, alters the phase-transition behavior of the diblocks (Figure 6B-C and Supplementary Figure S10). In this construct, stimuli exposure and cleavage of **1** or **2**—despite decreasing overall hydrophobicity—led to a reduction in the transition temperature. This counterintuitive result is again attributed to the presence of nanostructures, which modulate the phase-transition profile independently of bulk hydrophobicity. Notably, RLP_{60}(**2**×18)-ELP_{60}(WT) exhibited no change in the turbidity profile after 1 h of incubation with β-gal. Therefore, we tested longer incubation times of 24 and 48 hours. While extended incubation did lead to a more substantial change in the transition profile, complete reversion was not achieved even after 48 hours (Supporting Information, Figure S10C). Overall, more rapid and more pronounced changes in the phase transition were observed for RLP_{60}(**1**×18)-ELP_{60}(WT) than for RLP_{60}(**2**×18)-ELP_{60}(WT) following exposure to their respective stimuli. This suggests that while H_2O_2 can readily diffuse into the RLP-containing core, the larger β-galactosidase enzyme has limited access to the densely packed core block of these nanostructures.

Assessment of self-assembly by DLS confirmed nanostructure formation for both RLP_{60}(**1**×18)-ELP_{60}(WT) and RLP_{60}(**2**×18)-ELP_{60}(WT) at 37 °C (Figure 6, D-E), with a CMC of <5 μM for both constructs (Supplementary Figure S11). The larger apparent sizes observed compared to the ELP-only diblocks are consistent with their tendency to form worm-like micelles. To evaluate whether these structures disassemble upon stimulus exposure, we monitored changes in the DLS

View Article Online
DOI: 10.1039/D5TB01334H

spectra. Although some changes in the observed hydrodynamic size were observed for RLP_{60}(**1**×18)-ELP_{60}(WT) following incubation with 1 mM H_2O_2 for 1 hour, RLP_{60}(**2**×18)-ELP_{60}(WT) exhibited no or minimal changes after incubation with 5 mg/ml β-gal even after 24 h (Figure 6, D and E), further supporting the hypothesis that the large enzyme is unable to efficiently penetrate the densely packed RLP core of these nanostructures.

To validate these findings, cryo-TEM images were collected before and after stimuli application. Prior to treatment, both RLP_{60}(**1**×18)-ELP_{60}(WT) and RLP_{60}(**2**×18)-ELP_{60}(WT) generated long, worm-like micelles. Following exposure to their respective stimulus (1 mM H_2O_2 or 5 mg/ml β-gal for 1 or 24 h respectively), cryo-TEM revealed a marked reduction in detectable intact nanostructures for RLP_{60}(**1**×18)-ELP_{60}(WT), whereas RLP_{60}(**2**×18)-ELP_{60}(WT) exhibited a minor reduction in the appearance of nano-worms with some organic matter (likely the enzyme) also visible (Figure 6F-G). These observations are consistent with the phase transition behavior and DLS results described above.

View Article Online
DOI: 10.1039/D5TB01334H

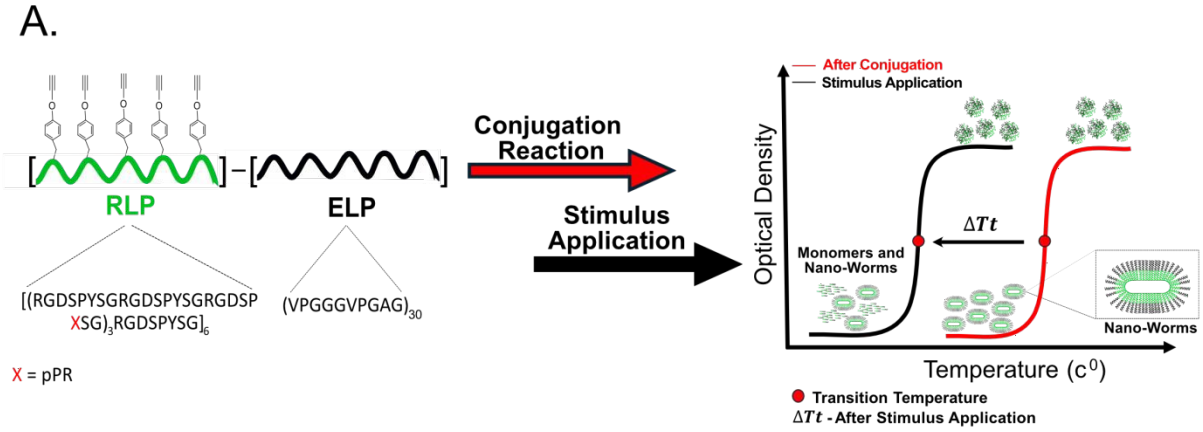

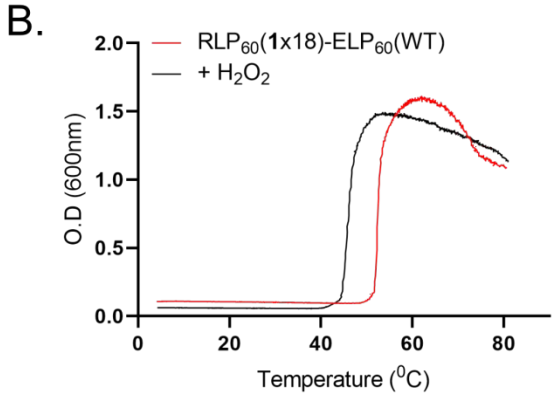

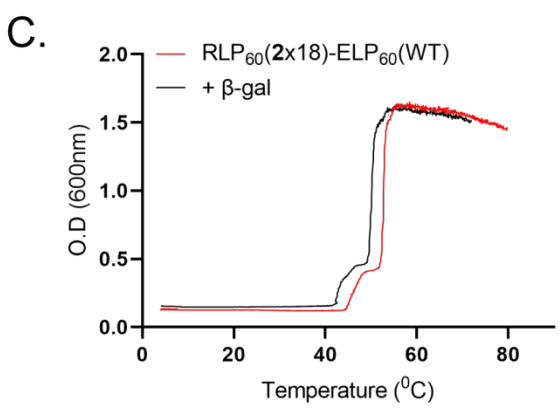

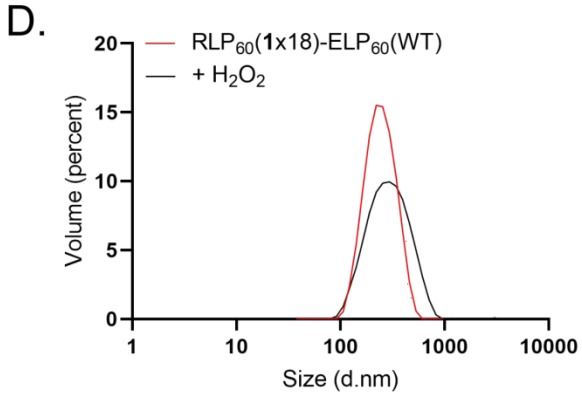

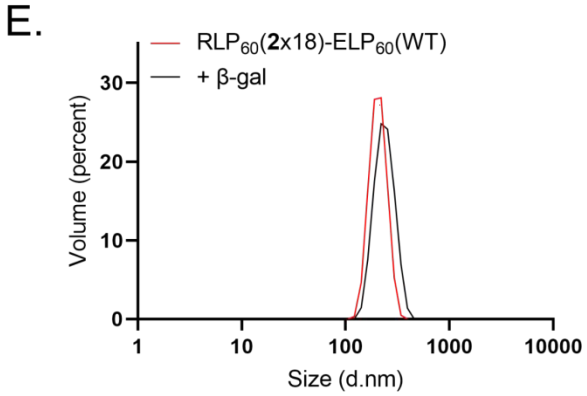

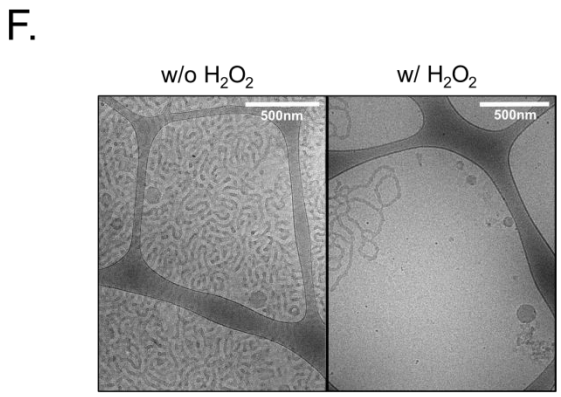

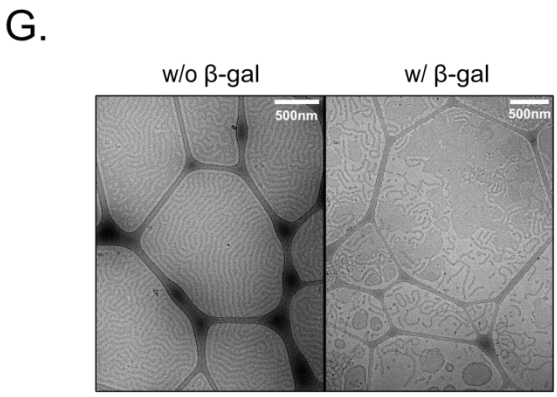

View Article Online
DOI: 10.1039/D5TB01334H

Figure 6. (A) Schematic illustration of turbidity and self-assembly changes in RLP_{60}(**pPR**×10)–ELP_{60}(WT) upon conjugation with molecule **1** or **2** and stimulus exposure. (B) Turbidity profiles as a function of temperature for RLP_{60}(**1**×10)–ELP_{60}(WT) before and after exposure to 1 mM H_2O_2 for 1 h (25 μM in PBS). (C) Turbidity profiles as a function of temperature for RLP_{60}(**2**×10)–ELP_{60}(WT) before and 24 h after exposure to 5 mg/mL β-gal (25 μM in PBS). (D) Observed Hydrodynamic radius of RLP_{60}(**1**×10)–ELP_{60}(WT) before and after exposure to 1 mM H_2O_2 for 1 h (25 μM in PBS, 37 °C). (E) Observed hydrodynamic radius of RLP_{60}(**2**×10)–ELP_{60}(WT) before and 24 h after exposure to 5 mg/mL β-gal (25 μM in PBS, 37 °C). (F) Cryo-TEM images of RLP_{60}(**1**×10)–ELP_{60}(WT) with and without exposure to 1 mM H_2O_2 for 1 h (25 μM in PBS, 37 °C), scale bar – 500nm. (G) Cryo-TEM images of RLP_{60}(**2**×10)–ELP_{60}(WT) with and without exposure to 5 mg/mL β-gal for 24 h (25 μM in PBS, 37 °C**),** scale bar – 500nm.

Finally, we evaluated the encapsulation and stimuli-responsive release capabilities of ELP-ELP and RLP-ELP nanostructures using Nile Red as a model hydrophobic compound. Nile Red is known to exhibit increased fluorescence when sequestered within hydrophobic environments, such as the cores of self-assembled nanostructures (Figure 7A). Indeed, a marked increase in the fluorescence of Nile Red (10 μM) was observed after 1 h incubation with both ELP_{60}(WT)–ELP_{60}(**1**×10) and RLP_{60}(**1**×18)–ELP_{60}(WT) (Figure 7B and D and Supplementary Figure S12-13). In contrast, the more hydrophilic ELP_{60}(WT)–ELP_{60}(**2**×10) and RLP_{60}(**2**×18)–ELP_{60}(WT) exhibited negligible fluorescence enhancement, indicating limited encapsulation (Supplementary Figure S12-13). Upon exposure to H_2O_2, a decrease in Nile Red fluorescence was observed, indicating its release from the hydrophobic cores of the nanostructures (Figure 7C and E and Supplementary Figure S12-14). The release profiles differed between the two systems and varied with H_2O_2 concentration. ELP-ELP micelles released ~70% of the encapsulated Nile Red within 1 h after exposure to 1 mM H_2O_2, compared to ~30% at 100 μM. In the absence of H_2O_2, the micelles effectively retained the dye, with less than 10% released over the same period. After 12 h, nearly all the dye (~90%) was released at 1 mM H_2O_2, while approximately 55% remained encapsulated at 100 μM. Under control conditions without H_2O_2, ~ 90% of the dye remained within the micelles even after 12 h, confirming the H_2O_2-dependent release mechanism.

View Article Online
DOI: 10.1039/D5TB01334H

In contrast, RLP-ELP nanoworms exhibited a slower release profile. In the presence of 1 mM H_2O_2, ~40% of the dye was released within the first hour, compared to just ~20% at 100 μM. In the absence of H_2O_2, the nanoworms also showed strong retention, with less than 10% release. After 12 h, the total release from the nanoworms at 1 mM H_2O_2 reached approximately 70%, while using 100 μM H_2O_2, the release plateaued at ~20% after 1 h, with no significant change over time. In the absence of H_2O_2, Nile Red fluorescence indicated that the nanoworms retained ~94% of the encapsulated dye over the entire 12-hour period. These results highlight the structural differences in nanocarrier stability and responsiveness to oxidative stimuli. Moreover, they strengthen the previously shown result that both the concentration and duration of stimulus exposure affect the morphological changes of the nanostructure, thus modulating the release of encapsulated cargo.

View Article Online
DOI: 10.1039/D5TB01334H

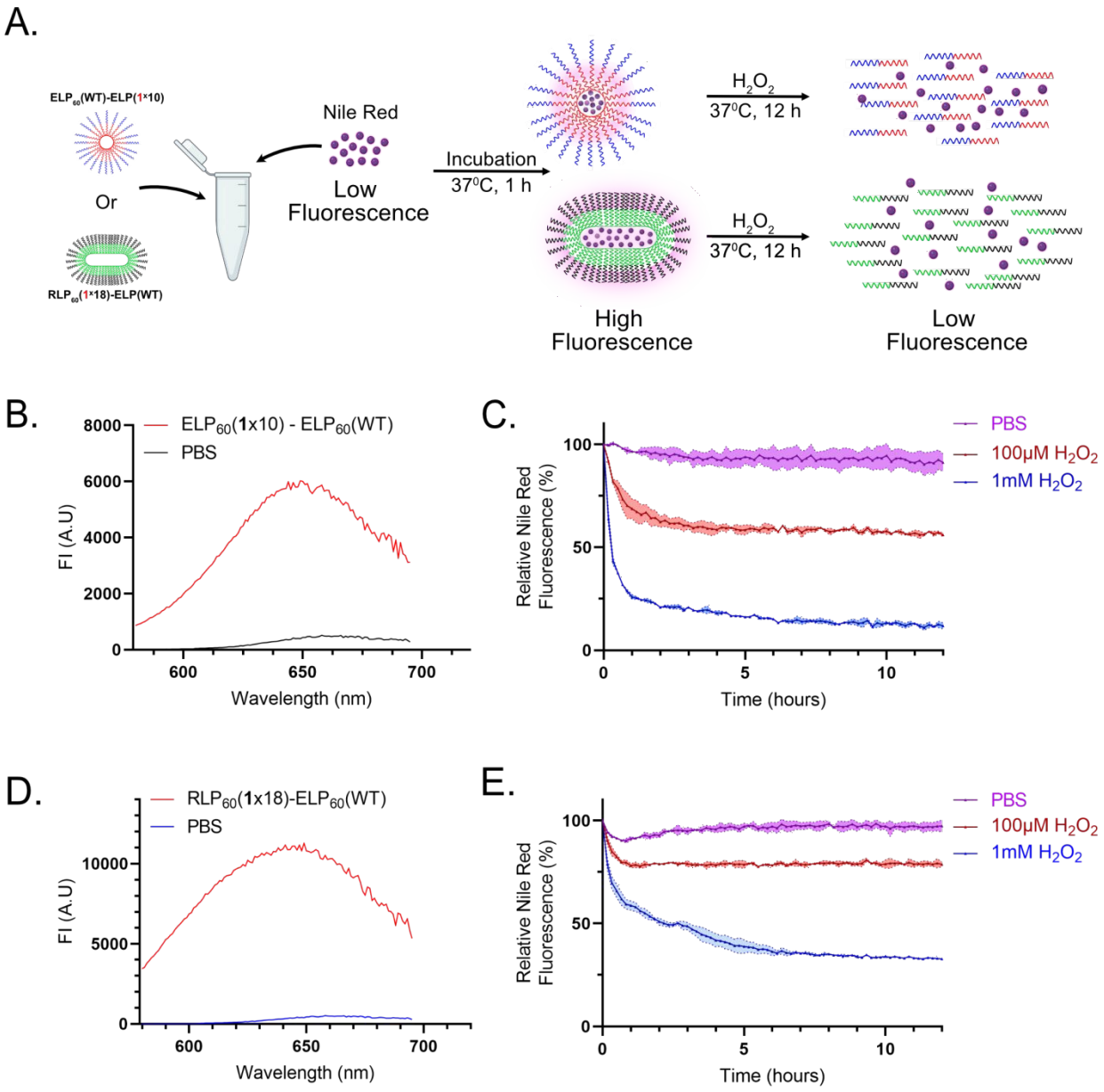

Figure 7. (A) Schematic illustration of Nile Red encapsulation by self-assembled ELP_{60}(WT)–ELP_{60}(**1**×10) or RLP_{60}(**1**×18)–ELP_{60}(WT), and the release of Nile Red upon stimulus exposure. **(B)** Fluorescence spectrum of ELP_{60}(WT)–ELP_{60}(**1**×10) (25 μM in PBS, 37 °C) after 1 h incubation with Nile Red vs. Nile Red in PBS. **(C)** Relative change in the fluorescence of Nile Red encapsulated in ELP_{60}(WT)–ELP_{60}(**1**×10) and incubated with PBS (control) or H_2O_2 (100 μM or 1 mM). (D) Fluorescence spectrum of RLP_{60}(**1**×18)–ELP_{60}(WT) (25 μM in PBS, 37 °C) after 1 h incubation with Nile Red vs. Nile Red in PBS. **(E)** Relative change in the fluorescence of Nile Red

View Article Online
DOI: 10.1039/D5TB01334H

encapsulated in RLP_{60}(**1**×18)–ELP_{60}(WT) and incubated with PBS (control) or H_2O_2 (100 μM or 1 mM). Error bars indicate average values ± SD.

Finally, we evaluated the stability and in vitro cytotoxicity of the nanostructures before and after exposure to stimuli. DLS analysis of RLP-ELP-based nanostructures in complete media (containing serum) confirmed their formation and stability, with consistent particle sizes observed in media for at least 48 hours (Supplementary Figure S15). In contrast, the smaller ELP-ELP-based nanostructures could not be reliably detected due to background interference from the media; however, similar ELP-ELP micelles have been reported both *in vitro* and *in vivo* [61-63]. Cytotoxicity was assessed in HEK cells incubated with up to 25 μM of the ELP-ELP or RLP-ELP constructs (Supplementary Figure S16). No significant loss of viability was observed across all nanostructure formulations. As expected, application of either stimulus induced some cytotoxicity. Interestingly, co-incubation of H_2O_2 with the nanostructures largely mitigated H_2O_2-induced toxicity, likely due to neutralization of the ROS via reaction with the conjugated head groups.

The concentration of ROS in cancer cells typically ranges from 50 to 100 μM. While several studies have investigated ROS-reactive polymeric carriers [42, 64, 65], relatively few focus on nano-assemblies for tumor-specific drug release within this range [66, 67]. For example, one study demonstrated nanoparticle disassembly after 48 hours of incubation with 100 μM hydrogen peroxide (H_2O_2) [68]. Another study reported a 50% release of the hydrophobic drug doxorubicin under similar conditions after 24 hours [67]. Similarly, a 50% reduction in Nile Red fluorescence—indicating release from the hydrophobic nanostructure core—was observed after 26 hours of exposure to either 100 μM or 1 mM H_2O_2, depending on the polymer design [66]. In a separate report, 60% of encapsulated Nile Red was released after 2 h of incubation with 100 μM H_2O_2 [69]. In this study, we demonstrate that ELP-based nano-assemblies, release ~40% of their cargo after 4 h incubation with 100 μM H_2O_2. In contrast, the RLP-ELP-based nanostructures exhibited a slower release profile, with only 20% of Nile Red released 1 h after exposure to 100 μM H_2O_2, based on Nile Red fluorescence measurements. We also observed that non-pathogenic levels of H_2O_2 (10 μM) do not induce nanoparticle disassembly, suggesting that drug release can be targeted to diseased sites. Taken together, these findings indicate that these ROS-sensitive nano-assemblies have potential as drug delivery vehicles responsive to pathophysiological ROS levels with tunable release profiles. Further enhancement of the system's sensitivity and release rate could be achieved by increasing the hydrophobicity change in the conjugated ELP or RLP block

View Article Online
DOI: 10.1039/D5TB01334H

upon H_2O_2 exposure—for example, by modifying the linker between the protein and the conjugated self-immolative molecule.

Although less explored in the previous literature, β-gal-responsive nanostructures [45, 46] hold significant therapeutic potential, particularly due to their ability to selectively target cellular environments with elevated β-gal expression—such as aging tissues or therapy-induced senescent tumor cells [44, 47, 70-72]. By engineering nanocarriers that degrade or release senolytic agents—compounds that preferentially induce cytotoxicity in senescent cells over healthy ones—in response to β-gal activity, enzyme-triggered, site-specific drug release can be achieved with minimal off-target effects and high therapeutic efficacy [45-47, 71, 72]. Future studies will investigate how carrier properties—such as nanostructure morphology, CMC, and the degree of β-gal responsiveness—influence drug efficacy and targeted delivery to senescent cells in both *in vitro* and *in vivo* models. Beyond drug delivery, β-gal-responsive nanostructures can also be engineered for diagnostic or theranostic applications through the conjugation of β-gal-responsive, self-immolative luminophores [73].

In this study, we employed an ELP-ELP and an RLP-ELP diblock to demonstrate that established design rules can be leveraged to impart novel stimuli-responsiveness to self-assembled nanoparticles using conjugation to self-immolative linkers [74, 75]. Of note, reported CMC values for other ELP-based diblocks range from 4-8 μM [18], suggesting that the conjugation of hydrophobic molecules, such as compound **1**, can be used to lower the CMC. This effect aligns with prior observations for ELP-drug and ELP-lipid conjugates [76, 77]. Numerous previous studies have demonstrated that varying the ratio of the hydrophobic and hydrophilic blocks, as well as the overall diblock length impacts the size and morphology of the self-assembled structures, critical micelle temperature (CMT), and Tt [27, 28, 74, 75]. Such modifications in block composition not only influence the architecture and stability of the self-assembled structures but also affect encapsulation efficiency and the release kinetics of encapsulated molecules, depending on their hydrophobicity [78]. Similar strategies could be applied to other natural proteins, whether ordered or intrinsically disordered, as well as synthetic polymers [23, 79], Genetically fused proteins or peptides can be displayed on the nanoparticle corona or encapsulated within the hydrophobic core, offering facile biological functionalization [23, 79]. Overall, a key advantage of our proposed approach is the precise control over key parameters such as hydrophobicity,

View Article Online
DOI: 10.1039/D5TB01334H

molecular weight, and the specific number and location of conjugation sites for stimuli-responsive chemical groups alongside facile biological functionalization via genetic fusion. Moving forward, these capabilities will enable the systematic variation of these factors to rationally design self-assembled morphologies and permit the fine-tuning of both their physicochemical and biological properties.

Conclusions

We report the successful generation of H_2O_2- and β-gal responsive ELPs via conjugation of self-immolative molecules that react with their respective stimulus. Libraries of single-block ELPs, decorated with alkyne moieties for site-specific conjugation were produced, and the effects of the number and identity of conjugated molecules, as well as stimulus exposure were examined. The results demonstrated that the number of conjugation sites can be used to tune the temperature range, with a window of up to 50 °C, within which stimulus exposure triggered the dissolution of phase-separated ELPs. Additionally, these single-block ELPs were incorporated into ELP-collagen-based hydrogels, where stimulus application was similarly shown to lower the ELP transition temperature, reducing the gel's optical density and enabling the controlled release of ELP from the hydrogel matrix. Finally, this concept was extended to the design of self-assembling diblock ELP-ELP and RLP-ELP, which disassembled upon stimulus exposure. The utility of such stimuli-responsive diblocks was demonstrated by their ability to encapsulate the hydrophobic dye Nile Red and release it under physiologically relevant H_2O_2 concentrations, highlighting their potential as stimuli-responsive drug delivery systems. Future studies will focus on evaluating the therapeutic potential of the H_2O_2- and β-gal-responsive hydrogels and nanostructures, including a comprehensive assessment of their stability and safety profiles, immunogenicity, and efficacy in relevant small animal models of cancer, inflammation, and aging.

This approach provides a general and versatile platform for introducing novel stimuli-responsive behaviors into elastin-like polypeptides (ELPs), resilin-like polypeptides (RLPs), and potentially other temperature-responsive protein-based polymers (PBPs) and IDPs. The creation of additional multi-block architectures using a variety of PBPs, and protein-PBP fusions can be attained by simply manipulating the genetic template, providing access to a diverse range of stimuli-responsive behaviors, self-assembled morphologies, and biologically active polymers. Moreover,

View Article Online
DOI: 10.1039/D5TB01334H

the conjugation of additional self-immolative molecules could broaden the range of stimuli to which these PBPs respond. Taken together, these template-directed yet chemically versatile PBPs can constitute a powerful platform for engineering smart biomaterials with programmable properties, suitable for applications such as targeted or biomolecule-responsive drug delivery, cell-responsive scaffolds, and biosensing.

View Article Online
DOI: 10.1039/D5TB01334H

Materials and methods

Protein expression and purification. Before batch expression, starter cultures (1:40 v/v of final expression volume) of 2xYT media, supplemented with kanamycin (30 μg ml^{-1}) and chloramphenicol (25 μg ml^{-1}), were inoculated with transformed cells from either a fresh agar plate or from stocks stored at −80 °C, incubated overnight at 34 °C while shaking at 220 rpm, and transferred to expression flasks containing 2xYT media, antibiotics, arabinose (0.2%), and pPR (1mM). Expression flasks were incubated at 34 °C for 4–5 h and then protein expression was induced with isopropyl β-d-1-thiogalactopyranoside (IPTG, 1 mM). The cells were harvested 24 h after inoculation by centrifugation at 4,000 g for 30 min at 4 °C. The cell pellet was then resuspended by vortex in milli-Q water (~4 ml) and either stored at −80 °C or purified immediately. For purification, resuspended pellets were lysed by ultrasonic disruption (18 cycles of 10 s sonication, separated by 40 s rest intervals). Poly(ethyleneimine) was added (0.2 ml of a 10% solution) to each lysed suspension before centrifugation at 4,000 g for 15 min at 4 °C to separate cell debris from the soluble cell lysate. All ELP constructs were purified by a modified inverse transition cycling (ITC) protocol[80] consisting of multiple "hot" and "cold" spins by using sodium chloride to trigger the phase transition. Before purification, the soluble cell lysate was incubated for 1–2 min at 42–55 °C to denature the native *E.coli* proteins. The cell lysate was then cooled on ice, centrifuged for 2 min at ~14,000 rpm, and the pellet was discarded. For "hot" spins, the ELP phase transition was triggered by adding sodium chloride to the cell lysate or to the product of a previous cycle of ITC at a final concentration of ~5 M. The solutions were then centrifuged at ~14,000 rpm for 10 min, and the pellets were resuspended in milli-Q water, after which a 2 min "cold" spin was performed without sodium chloride to remove the denatured contaminants. Additional rounds of ITC were conducted as needed using a saturated sodium chloride solution until sufficient purification was achieved. Purified proteins were visualized on SDS-PAGE.

Protein conjugation. Proteins bearing alkyne groups were reacted with azide-bearing self-immolative molecules **1** or **2** using copper-catalyzed azide-alkyne cycloaddition. For this reaction, proteins and reagents were diluted and mixed using the concentrations indicated in the table below for each ELP:

View Article Online
DOI: 10.1039/D5TB01334H

Construct	ELP (μM)	Cargo-azide	$CuSO_4$ (μM)*	THPTA (μM)*	aminoguanidine hydrochloride (mM)	sodium ascorbate (mM)
ELP_{60}(**pPR**×2)	5	50	40	80	5	5
ELP_{60}(**pPR**×4)	5	100	80	160	5	5
ELP_{60}(**pPR**×6)	5	150	120	240	5	5
ELP_{60}(**pPR**×10)	5	250	200	400	5	5
ELP_{60}(WT)-ELP_{60}(**pPR**×10)	5	250	200	400	5	5
RLP_{60}(**pPR**×18)-ELP_{60}(WT)	5	450	360	720	5	5

*CuSO4 and THPTA were pre-mixed for 20 min.

The reaction was performed for 2 h at 34 °C in a shaking incubator (220 rpm) in the dark. After incubation, EDTA was added at a 1:5 ratio of EDTA to copper, and buffer exchange was performed using Amicon filters (10 kDa MWCO).

Intact mass measurements. The intact mass was measured using MALDI-TOF/TOF autoflex speed at the Ilse Katz Institute for Nanoscale Science and Technology (Ben-Gurion University of the Negev). Spectrum analysis was performed by the Flexanalysis software.

Phase transition analysis. To characterize the inverse transition temperature of the PBPs variants, samples were incubated for 1 h with the respective stimuli at indicated concentrations (at 25^0c and 37^0c for **1** and **2** respectively), then the $O.D_{600}$ of the ELP solution (in PBS, unless otherwise noted) was monitored as a function of temperature, with heating and cooling performed at a rate of 1 °C min^{-1} on a UV-vis spectrophotometer equipped with a multicell thermoelectric temperature controller (Thermo Scientific).

Dynamic light scattering (DLS) analysis. Diblock self-assembly was analyzed using a Zetasizer Nano ZS (Malvern Panalytical). For each sample, 12–17 acquisitions (determined automatically by the instrument) were obtained. The temperature was adjusted depending on the transition temperature of the examined ELPs. The CMC was determined at 37 °C by varying the ELP

View Article Online
DOI: 10.1039/D5TB01334H

concentration. Populations comprising less than 1% of the total mass (by volume) were excluded from the analysis.

Preparation of collagen and ELP-collagen hydrogels. Collagen type I (Corning® Collagen I, Rat Tail) and ELP_{60}(**1**×6) and ELP_{60}(**2**×10) were used to create control and stimuli-responsive hydrogels with the following compositions: (i) 1 mg/ml collagen, (ii) 60 μM ELP_{60}(**1**×6) and 1 mg/ml collagen, and (iii) 30 μM ELP_{60} (**2**×10) and 1 mg/ml collagen. The standard manufacturer's protocol for collagen gel formation was followed with slight modifications. Briefly, sterile deionized water (DI), 10× PBS, 1 N NaOH, and collagen stock solution (9.54 mg/ml) were used to prepare a collagen solution at 2 mg/ml in 1× PBS. The collagen solution was gently mixed with ELP stock solutions in PBS or with PBS alone. For hydrogel visualization, 300 μl of each solution was transferred to a 1.5 ml glass vial. The hydrogel solutions were incubated for 2 hours at 37 °C to promote gelation before adding PBS or trigger solutions at a 1:1 volume ratio with the hydrogels. For ELP_{60}(**1**×6)-collagen hydrogels, 1 mM of H_2O2 in PBS, or PBS, were added. For ELP_{60}(**2**×10)-collagen hydrogels, 5 mg/ml of β-gal in PBS, or PBS, were added. Images of the gels were taken 24 h after incubation in the respective solutions.

Hydrogel optical density measurements. Collagen-ELP hydrogel solutions were prepared as described above. A 150 μl volume of hydrogel solution was transferred to a 96-well plate and incubated for 2 hours at 37 °C to promote gelation. After incubation, PBS or trigger solutions were added to the hydrogel solutions at a 1:1 volume ratio. For ELP_{60}(**1**×6)-collagen hydrogels, 1 mM or 10 mM H_2O_2 in PBS, or PBS (control), were added. For ELP_{60}(**2**×10)-collagen hydrogels, 5 mg/ml or 0.5 mg/ml β-gal in PBS, or PBS (control), were added. Optical density was measured at 600 nm using a Biotek spectrophotometric plate reader for up to 48 hours.

Evaluation of ELP release from hydrogels

Collagen-ELP hydrogel solutions were prepared as described above and incubated for 24 hours with either PBS, 100 μM or 1 mM H_2O_2 (for ELP_{60}(**1**×6)-collagen hydrogels), or 5 mg/mL and 0.5 mg/mL β-gal (for ELP_{60}(**2**×10)-collagen hydrogels). At several time points, 15 μL of solution from the surroundings of each hydrogel was collected. Each sample was mixed with 5 μL of 4× Laemmli sample buffer and heated to 95 °C for 5 minutes. Then, 9 μL of each sample was loaded

View Article Online
DOI: 10.1039/D5TB01334H

onto a 12% SDS-PAGE gel and stained using Imidazole-Zinc inverse staining or Instant Blue, as indicated.

Rheology Measurements. The rheological measurements were carried out on an Anton Paar MCR 702 rheometer (Graz, Austria) using a sandblasted parallel plate geometry (with a diameter of 25 mm). A strain amplitude sweep was carried out at 10 rad/s and 37 °C, to determine the strain values corresponding to the upper limit of the linear viscoelastic (LVE) range. Subsequently, the sample was subjected to a constant strain at 1 percent in the LVE region, the frequency was conducted between 0.1 and 10 radians per second, and the shear stress was recorded.

Transmission electron microscopy. TEM at cryogenic temperature (Cryo-TEM) was used for imaging of the hydrogels. Vitrified specimens were prepared on a copper grid coated with a perforated lacey carbon 300 mesh (Ted Pella Inc.). A few microliters from the gel were applied to the grid and blotted with a filter paper to form a thin liquid film of solution. The blotted sample were immediately plunged into liquid ethane at its freezing point (-183°C). The procedure was performed automatically in the Plunger (Lieca EM GP). The vitrified specimens were then transferred into liquid nitrogen for storage. The samples were studied using a FEI Talos F200C TEM, at 200kV maintained at -180 °C; and images are recorded on a FEI Ceta 16M camera (4k × 4k CMOS sensor) at low dose conditions, to minimize electron beam radiation damage. The measurements were done at the Ilse Katz Institute for Nanoscale Science and Technology (Ben-Gurion University of the Negev).

Nile Red encapsulation and fluorescence Analysis. The encapsulation of Nile Red and subsequent fluorescence analysis were carried out based on a previously reported protocol with slight modifications [76, 81]. Nile Red was mixed with either ELP_{60}(WT)–ELP_{60}(**1** or **2**×10) or RLP_{60}(**1** or **2**×18)–ELP_{60}(WT), yielding final concentrations of 10 μM Nile Red and 12 μM or 25 μM protein in PBS, respectively. Samples were incubated for 1 hour at 37 °C with gentle shaking (400 rpm). Fluorescence spectra were measured using a BioTek plate reader with excitation at 550 nm and emission recorded from 580 to 750 nm. For kinetic measurements, Stimuli were applied by adding H_2O_2 to final concentrations of 100 μM or 1 mM, with PBS-treated

View Article Online
DOI: 10.1039/D5TB01334H

samples serving as controls. A 150 μL aliquot of each sample was transferred to a 96-well plate, and fluorescence intensity at 626 nm (excitation at 550 nm) was monitored over 12 hours.

In vitro cytotoxicity. Human embryonic kidney (HEK293) cells were used to study the *in vitro* cytotoxicity of the nanostructure-conjugates before and after stimuli exposure. Cells were grown as monolayer at 37 °C with CO_2 in a humidified incubator in DMEM medium supplemented with 10% FBS and 1% penicillin-streptomycin. For cytotoxicity assay, $1 \cdot 10^4$ cells were seeded per well in a 96-well plate and were allowed to grow for 24 hrs. Then, the medium was removed and replaced with medium containing ELP–ELP and RLP–ELP polymers conjugated with molecules 1 and 2, with or without pre-incubation (2 h) with the corresponding triggers, before adding to the cells. After 24 of treatment, the viability of cells was determined using XTT cell proliferation kit, by the addition of XTT and activation reagents to the medium. After 2 hrs incubation at 37 °C with CO_2 in a humidified incubator, the absorbance at 450 nm was measured using a Biotek spectrophotometric plate reader. Absorbance at 450 nm was corrected by subtracting the absorbance at 450 nm of medium without cells. Cell viability was defined as the percentage of the absorbance of treated cells relative to control PBS-treated cells.

Statistical Analysis. For statistical analyses involving multiple group comparisons, one-way ANOVA was performed followed by Dunnett's post hoc test for comparisons against a specified control group or Tukey's post hoc test for comparisons among all groups, with $p < 0.05$ considered statistically significant. All analyses assumed a Gaussian distribution with unequal variances.

View Article Online
DOI: 10.1039/D5TB01334H

Data availability statement

The data supporting this article have been included as part of the Supplementary Information.

Funding

This work was funded by the European Research Council (ERC) under the European Union's Horizon 2020 Research and Innovation program, grant agreement 756996 and the Israel Science Foundation (grant number 939\21) (to M.A). We also gratefully acknowledge support from the Avram and Stella Goldstein-Goren fund.

Conflict of interest statement

There are no conflicts of interest to declare

Acknowledgments

We thank Dr. Mark Karpasas from the Ilse Katz Institute for Nanoscale Science & Technology for the professional help with the mass spectrometry experiments and Dr. Einat Nativ-Roth from the Ilse Katz Institute for Nanoscale Science & Technology for her professional help with the cryo-TEM experiments. Figures were partially created with Biorender.com

View Article Online
DOI: 10.1039/D5TB01334H

References

1. Mamidi, N., F. Franco De Silva, and A. Orash Mahmoudsalehi, *Advanced disease therapeutics using engineered living drug delivery systems.* Nanoscale, 2025. **17**(13): p. 7673-7696.
2. Li, Y., et al., *Design of Stimuli-Responsive Peptides and Proteins.* Advanced Functional Materials, 2023. **33**(7).
3. Martínez-Orts, M. and S. Pujals, *Responsive Supramolecular Polymers for Diagnosis and Treatment.* International Journal of Molecular Sciences, 2024. **25**(7): p. 4077.
4. Giraldo-Castano, M.C., et al., *Programmability and biomedical utility of intrinsically-disordered protein polymers.* Adv Drug Deliv Rev, 2024. **212**: p. 115418.
5. Varanko, A., S. Saha, and A. Chilkoti, *Recent trends in protein and peptide-based biomaterials for advanced drug delivery.* Adv Drug Deliv Rev, 2020. **156**: p. 133-187.
6. Garcia Garcia, C., et al., *Recombinant protein-based injectable materials for biomedical applications.* Adv Drug Deliv Rev, 2023. **193**: p. 114673.
7. Saurav, S., et al., *Harnessing Natural Polymers for Nano-Scaffolds in Bone Tissue Engineering: A Comprehensive Overview of Bone Disease Treatment.* Current Issues in Molecular Biology, 2024. **46**(1): p. 585-611.
8. Phan, A. and J.A. MacKay, *Steric stabilization of bioactive nanoparticles using elastin-like polypeptides.* Adv Drug Deliv Rev, 2024. **206**: p. 115189.
9. Mamidi, N., et al., *Innovative hydrogel-based delivery systems for immunotherapy: A review of pre-clinical progress.* Nano Research, 2024. **17**(10): p. 9031-9043.
10. Mamidi, N., et al., *Multifaceted Hydrogel Scaffolds: Bridging the Gap between Biomedical Needs and Environmental Sustainability.* Advanced Healthcare Materials, 2024. **13**(27).
11. Varanko, A.K., J.C. Su, and A. Chilkoti, *Elastin-Like Polypeptides for Biomedical Applications.* Annu Rev Biomed Eng, 2020. **22**: p. 343-369.
12. Acosta, S., et al., *Elastin-Like Recombinamers: Deconstructing and Recapitulating the Functionality of Extracellular Matrix Proteins Using Recombinant Protein Polymers.* Advanced Functional Materials, 2020. **30**(44).
13. Milligan, J.J., et al., *Genetically encoded elastin-like polypeptide nanoparticles for drug delivery.* Current Opinion in Biotechnology, 2022. **74**.
14. Israeli, B., et al., *Genetically Encoding Light-Responsive Protein-Polymers Using Translation Machinery for the Multi-Site Incorporation of Photo-Switchable Unnatural Amino Acids.* Advanced Functional Materials, 2021. **31**(44).
15. Strugach, D.S., D. Hadar, and M. Amiram, *Robust Photocontrol of Elastin-like Polypeptide Phase Transition with a Genetically Encoded Arylazopyrazole.* ACS Synth Biol, 2023. **12**(10): p. 2802-2811.
16. Wang, Q., et al., *High Throughput Screening of Dynamic Silk-Elastin-Like Protein Biomaterials.* Adv Funct Mater, 2014. **24**(27): p. 4303-4310.
17. Mackay, J.A., et al., *Quantitative model of the phase behavior of recombinant pH-responsive elastin-like polypeptides.* Biomacromolecules, 2010. **11**(11): p. 2873-9.
18. Dreher, M.R., et al., *Temperature triggered self-assembly of polypeptides into multivalent spherical micelles.* Journal of the American Chemical Society, 2008. **130**(2): p. 687-694.
19. Fluegel, S., et al., *Self-assembly of monodisperse oligonucleotide-elastin block copolymers into stars and compound micelles.* Chemistry, 2011. **17**(20): p. 5503-6.
20. Garcia Quiroz, F., et al., *Intrinsically disordered proteins access a range of hysteretic phase separation behaviors.* Sci Adv, 2019. **5**(10): p. eaax5177.
21. Saha, S., et al., *Engineering the Architecture of Elastin-Like Polypeptides: From Unimers to Hierarchical Self-Assembly.* Advanced Therapeutics, 2020. **3**(3).

View Article Online
DOI: 10.1039/D5TB01334H

22. Schreiber, A., et al., *Self-Assembly Toolbox of Tailored Supramolecular Architectures Based on an Amphiphilic Protein Library.* Small, 2019. **15**(30): p. e1900163.
23. Quintanilla-Sierra, L., C. Garcia-Arevalo, and J.C. Rodriguez-Cabello, *Self-assembly in elastin-like recombinamers: a mechanism to mimic natural complexity.* Mater Today Bio, 2019. **2**: p. 100007.
24. Janib, S.M., et al., *A quantitative recipe for engineering protein polymer nanoparticles.* Polymer Chemistry, 2014. **5**(5): p. 1614-1625.
25. Balu, R., et al., *Resilin-mimetics as a smart biomaterial platform for biomedical applications.* Nature Communications, 2021. **12**(1).
26. Gueta, O., et al., *Tuning the Properties of Protein-Based Polymers Using High-Performance Orthogonal Translation Systems for the Incorporation of Aromatic Non-Canonical Amino Acids.* Front Bioeng Biotechnol, 2022. **10**: p. 913057.
27. Weitzhandler, I., et al., *Micellar Self-Assembly of Recombinant Resilin-/Elastin-Like Block Copolypeptides.* Biomacromolecules, 2017. **18**(8): p. 2419-2426.
28. Basheer, A., et al., *Switchable Self-Assembly of Elastin- and Resilin-Based Block Copolypeptides with Converse Phase Transition Behaviors.* Acs Applied Materials & Interfaces, 2021. **13**(21): p. 24385-24400.
29. Azulay, R., D.S. Strugach, and M. Amiram, *Self-assembly of temperature-responsive di-block polypeptides functionalized with unnatural amino acids.* Protein Science, 2024. **33**(2).
30. Dzuricky, M., et al., *De novo engineering of intracellular condensates using artificial disordered proteins.* Nat Chem, 2020. **12**(9): p. 814-825.
31. Gnaim, S. and D. Shabat, *Self-Immolative Chemiluminescence Polymers: Innate Assimilation of Chemiexcitation in a Domino-like Depolymerization.* Journal of the American Chemical Society, 2017. **139**(29): p. 10002-10008.
32. Sagi, A., et al., *Self-immolative polymers.* Journal of the American Chemical Society, 2008. **130**(16): p. 5434-+.
33. Shelef, O., S. Gnaim, and D. Shabat, *Self-Immolative Polymers: An Emerging Class of Degradable Materials with Distinct Disassembly Profiles.* Journal of the American Chemical Society, 2021. **143**(50): p. 21177-21188.
34. Zhang, L., et al., *Cellular senescence: a key therapeutic target in aging and diseases.* Journal of Clinical Investigation, 2022. **132**(15).
35. Li, X.Y., et al., *Targeting mitochondrial reactive oxygen species as novel therapy for inflammatory diseases and cancers.* Journal of Hematology & Oncology, 2013. **6**.
36. Hadar, D., et al., *Efficient Incorporation of Clickable Unnatural Amino Acids Enables Rapid and Biocompatible Labeling of Proteins in Vitro and in Bacteria.* Chembiochem, 2021. **22**(8): p. 1379-1384.
37. Zhang, Y., et al., *A PEGylated alternating copolymer with oxidation-sensitive phenylboronic ester pendants for anticancer drug delivery.* Biomaterials Science, 2019. **7**(9): p. 3898-3905.
38. Gueta, O., et al., *Tuning the Properties of Protein-Based Polymers Using High-Performance Orthogonal Translation Systems for the Incorporation of Aromatic Non-Canonical Amino Acids.* Frontiers in Bioengineering and Biotechnology, 2022. **10**: p. 913057.
39. McDaniel, J.R., D.C. Radford, and A. Chilkoti, *A Unified Model for Design of Elastin-like Polypeptides with Tunable Inverse Transition Temperatures.* Biomacromolecules, 2013. **14**(8): p. 2866-2872.
40. de Haas, R.J., et al., *pH-Responsive Elastin-Like Polypeptide Designer Condensates.* ACS Appl Mater Interfaces, 2023. **15**(38): p. 45336-45344.

View Article Online
DOI: 10.1039/D5TB01334H

41. Hassouneh, W., et al., *Calcium binding peptide motifs from calmodulin confer divalent ion selectivity to elastin-like polypeptides.* Biomacromolecules, 2013. **14**(7): p. 2347-53.
42. Wang, J.Q., et al., *Leveraging H*

O

Levels for Biomedical Applications. Advanced Biosystems, 2017. **1**(9).
43. Hu, X.L., et al., *H*

O

-Responsive Vesicles Integrated with Transcutaneous Patches for Glucose-Mediated Insulin Delivery. Acs Nano, 2017. **11**(1): p. 613-620.
44. Li, M., M.Q. Yang, and W.H. Zhu, *Advances in fluorescent sensors for β-galactosidase.* Materials Chemistry Frontiers, 2021. **5**(2): p. 763-774.
45. Parshad, B., et al., *Improved Therapeutic Efficiency of Senescent Cell-specific, Galactose-Functionalized Micelle Nanocarriers.* Small, 2025. **21**(7).
46. Munoz-Espin, D., et al., *A versatile drug delivery system targeting senescent cells.* EMBO Mol Med, 2018. **10**(9).
47. González-Gualda, E., et al., *Galacto-conjugation of Navitoclax as an efficient strategy to increase senolytic specificity and reduce platelet toxicity.* Aging Cell, 2020. **19**(4).
48. Shelef, O., S. Gnaim, and D. Shabat, *Self-Immolative Polymers: An Emerging Class of Degradable Materials with Distinct Disassembly Profiles.* J Am Chem Soc, 2021. **143**(50): p. 21177-21188.
49. Xiao, Y., et al., *Self-immolative polymers in biomedicine.* J Mater Chem B, 2020. **8**(31): p. 6697-6709.
50. Meco, E. and K.J. Lampe, *Impact of Elastin-like Protein Temperature Transition on PEG-ELP Hybrid Hydrogel Properties.* Biomacromolecules, 2019. **20**(5): p. 1914-1925.
51. Lee, K., et al., *Tunable Physicomechanical and Drug Release Properties of In Situ Forming Thermoresponsive Elastin-like Polypeptide Hydrogels.* Biomacromolecules, 2022. **23**(12): p. 5193-5201.
52. Sharma, A., P. Sharma, and S. Roy, *Elastin-inspired supramolecular hydrogels: a multifaceted extracellular matrix protein in biomedical engineering.* Soft Matter, 2021. **17**(12): p. 3266-3290.
53. Dragojevic, S., et al., *Elastin-like Polypeptide Hydrogels for Tunable, Sustained Local Chemotherapy in Malignant Glioma.* Pharmaceutics, 2022. **14**(10).
54. Gurumurthy, B., P.C. Bierdeman, and A.V. Janorkar, *Composition of elastin like polypeptide–collagen composite scaffold influences in vitro osteogenic activity of human adipose derived stem cells.* Dental Materials, 2016. **32**(10): p. 1270-1280.
55. Pal, P., et al., *Drug-Loaded Elastin-Like Polypeptide-Collagen Hydrogels with High Modulus for Bone Tissue Engineering.* Macromol Biosci, 2019. **19**(9): p. e1900142.
56. Anguiano, M., et al., *Characterization of three-dimensional cancer cell migration in mixed collagen-Matrigel scaffolds using microfluidics and image analysis.* PLoS One, 2017. **12**(2): p. e0171417.
57. Motte, S. and L.J. Kaufman, *Strain stiffening in collagen I networks.* Biopolymers, 2013. **99**(1): p. 35-46.
58. El-Husseiny, H.M., et al., *Smart/stimuli-responsive hydrogels: Cutting-edge platforms for tissue engineering and other biomedical applications.* Materials Today Bio, 2022. **13**.
59. Neumann, M., et al., *Stimuli-Responsive Hydrogels: The Dynamic Smart Biomaterials of Tomorrow.* Macromolecules, 2023. **56**(21): p. 8377-8392.

View Article Online
DOI: 10.1039/D5TB01334H

60. Amruthwar, S.S., A.D. Puckett, and A.V. Janorkar, *Preparation and characterization of novel elastin-like polypeptide-collagen composites.* J Biomed Mater Res A, 2013. **101**(8): p. 2383-91.
61. Dhandhukia, J.P., et al., *Bifunctional Elastin-like Polypeptide Nanoparticles Bind Rapamycin and Integrins and Suppress Tumor Growth in Vivo.* Bioconjug Chem, 2017. **28**(11): p. 2715-2728.
62. Sarangthem, V., et al., *Effects of molecular weight and structural conformation of multivalent-based elastin-like polypeptides on tumor accumulation and tissue biodistribution.* Nanotheranostics, 2020. **4**(2): p. 57-70.
63. Simnick, A.J., et al., *In vivo tumor targeting by a NGR-decorated micelle of a recombinant diblock copolypeptide.* J Control Release, 2011. **155**(2): p. 144-51.
64. Song, C.C., et al., *Oxidation-Responsive Poly(amino ester)s Containing Arylboronic Ester and Self-Immolative Motif: Synthesis and Degradation Study.* Macromolecules, 2013. **46**(21): p. 8416-8425.
65. Ge, C.L., et al., *ROS-Responsive Selenopolypeptide Micelles: Preparation, Characterization, and Controlled Drug Release.* Biomacromolecules, 2022. **23**(6): p. 2647-2654.
66. de Gracia Lux, C., et al., *Biocompatible polymeric nanoparticles degrade and release cargo in response to biologically relevant levels of hydrogen peroxide.* J Am Chem Soc, 2012. **134**(38): p. 15758-64.
67. Wang, K., et al., *Self-immolative polyprodrug-based tumor-specific cascade amplificated drug release nanosystem for orchestrated synergistic cancer therapy.* Biomaterials, 2022. **289**: p. 121803.
68. Phan, H., et al., *H2O2-Responsive Nanocarriers Prepared by RAFT-Mediated Polymerization-Induced Self-Assembly of N-(2-(Methylthio)ethyl)acrylamide for Biomedical Applications.* Acs Applied Polymer Materials, 2022.
69. Kim, A.Y., J.H. Ha, and S.N. Park, *Selective Release System for Antioxidative and Anti-Inflammatory Activities Using H*

O

-Responsive Therapeutic Nanoparticles. Biomacromolecules, 2017. **18**(10): p. 3197-3206.
70. Gu, K.Z., et al., *Real-Time Tracking and In Vivo Visualization of β-Galactosidase Activity in Colorectal Tumor with a Ratiometric Near-Infrared Fluorescent Probe.* Journal of the American Chemical Society, 2016. **138**(16): p. 5334-5340.
71. Sharma, A., et al., *Development of a theranostic prodrug for colon cancer therapy by combining ligand-targeted delivery and enzyme-stimulated activation.* Biomaterials, 2018. **155**: p. 145-151.
72. Cai, Y., et al., *Elimination of senescent cells by beta-galactosidase-targeted prodrug attenuates inflammation and restores physical function in aged mice.* Cell Res, 2020. **30**(7): p. 574-589.
73. Gnaim, S., et al., *Direct Real-Time Monitoring of Prodrug Activation by Chemiluminescence.* Angew Chem Int Ed Engl, 2018. **57**(29): p. 9033-9037.
74. Meyer, D.E. and A. Chilkoti, *Genetically encoded synthesis of protein-based polymers with precisely specified molecular weight and sequence by recursive directional ligation: examples from the elastin-like polypeptide system.* Biomacromolecules, 2002. **3**(2): p. 357-67.
75. Janib, S.M., et al., *A quantitative recipe for engineering protein polymer nanoparticles.* Polym Chem, 2014. **5**(5): p. 1614-1625.
76. Zhang, T., et al., *Solution behavior and encapsulation properties of fatty acid-elastin-like polypeptide conjugates.* RSC Adv, 2023. **13**(3): p. 2190-2201.

View Article Online
DOI: 10.1039/D5TB01334H

77. McDaniel, J.R., et al., *Self-assembly of thermally responsive nanoparticles of a genetically encoded peptide polymer by drug conjugation.* Angew Chem Int Ed Engl, 2013. **52**(6): p. 1683-7.
78. Iqbal, S., et al., *Carriers for hydrophobic drug molecules: lipid-coated hollow mesoporous silica particles, and the influence of shape and size on encapsulation efficiency.* Nanoscale, 2024. **16**(23): p. 11274-11289.
79. Saha, S., et al., *Engineering the Architecture of Elastin-Like Polypeptides: From Unimers to Hierarchical Self-Assembly.* Adv Ther (Weinh), 2020. **3**(3).
80. Hassouneh, W., T. Christensen, and A. Chilkoti, *Elastin-like polypeptides as a purification tag for recombinant proteins.* Curr Protoc Protein Sci, 2010. **Chapter 6**: p. Unit 6 11.
81. Parshad, B., et al., *Improved Therapeutic Efficiency of Senescent Cell-specific, Galactose-Functionalized Micelle Nanocarriers.* Small, 2025. **21**(7): p. e2405732.

View Article Online
DOI: 10.1039/D5TB01334H

Data availability statement

The data supporting this article have been included as part of the Supplementary Information.